A peer-reviewed version of this preprint was published in PeerJ on 20 October 2016.

View the peer-reviewed version (peerj.com/articles/2607), which is the preferred citable publication unless you specifically need to cite this preprint.

Labra FA, Bogdanovich JM, Bozinovic F. 2016. Nonlinear temperature effects on multifractal complexity of metabolic rate of mice. PeerJ 4:e2607 https://doi.org/10.7717/peerj.2607

Nonlinear temperature effects on multifractal complexity of metabolic rate of mice

Fabio A Labra Corresp., [1, 2] , **Jose M Bogdanovich** [2, 3] , **Francisco Bozinovic** [3]

[1] Facultad de Ciencias, Universidad Santo Tomás, Santiago, Chile

[2] Centro de Investigación e Innovación para el Cambio Climático, Universidad Santo Tomás, Santiago, Chile

[3] Departamento de Ecología, Center of Applied Ecology & Sustainability (CAPES) and LINC-Global, Facultad de Ciencias Biológicas, Pontificia Universidad Católica de Chile, Santiago, Chile

Corresponding Author: Fabio A Labra
Email address: flabra@santotomas.cl

Complex physiological dynamics have been argued to be a signature of healthy physiological function. Here we test whether the complexity of metabolic rate fluctuations in small endotherms decreases with lower environmental temperatures. To do so we examine the multifractal temporal scaling properties of the rate of change in oxygen consumption $r(VO_2)$, in the laboratory mouse *Mus musculus*, assessing their long range correlation properties across 7 different environmental temperatures, ranging from 0°C to 30°C. To do so, we applied multifractal detrended fluctuation analysis (MF-DFA), finding that $r(VO_2)$ fluctuations show two scaling regimes. For small time scales below the crossover time (approximately 10^2 seconds), either monofractal or weak multifractal dynamics are observed depending on whether T_a<15°C or T_a > 15°C respectively. For larger time scales, $r(VO_2)$ fluctuations are characterized by an asymptotic scaling exponent that indicates multifractal anti-persistent or uncorrelated dynamics. For both scaling regimes, a generalization of the multiplicative cascade model provides very good fits for the Renyi exponents $\tau(q)$, showing that the infinite number of exponents $h(q)$ can be described by only two independent parameters, a and b. We also show that the long-range correlation structure of $r(VO_2)$ time series differs from randomly shuffled series, and may not be explained as an artifact of stochastic sampling of a linear frequency spectrum. These results show that metabolic rate dynamics in a well studied micro-endotherm are consistent with a highly non-linear feedback control system.

Nonlinear temperature effects on multifractal complexity of metabolic rate of mice

Fabio A. Labra[1,2], José M. Bogdanovich[2,3,**] and Francisco Bozinovic[3*].

[1]Facultad de Ciencias, Universidad Santo Tomas, Ejercito 146, Código Postal 8370003, Santiago, Chile.

[2]Centro de Investigación e Innovación para el Cambio Climático (CIICC), Universidad Santo Tomás, Ejercito 146, Código Postal 8370003, Santiago, Chile..

[3]Departamento de Ecología, Center of Applied Ecology & Sustainability (CAPES) and LINC-Global, Facultad de Ciencias Biológicas, Pontificia Universidad Católica de Chile, Código Postal 6513677, Chile.

*Corresponding Author;

Fabio A. Labra[1,2]

Ejército 146, Código Postal 8370003, Santiago, Chile

Email address: flabra@santotomas.cl

**Former José M. Rojas

Abstract

Complex physiological dynamics have been argued to be a signature of healthy physiological function. Here we test whether the complexity of metabolic rate fluctuations in small endotherms decreases with lower environmental temperatures. To do so we examine the multifractal temporal scaling properties of the rate of change in oxygen consumption $r(VO_2)$, in the laboratory mouse *Mus musculus*, assessing their long range correlation properties across 7 different environmental temperatures, ranging from 0°C to 30°C. To do so, we applied multifractal detrended fluctuation analysis (MF-DFA), finding that $r(VO_2)$ fluctuations show two scaling regimes. For small time scales below the crossover time (approximately 10^2 seconds), either monofractal or weak multifractal dynamics are observed depending on whether T_a<15°C or T_a≥15°C respectively. For larger time scales, $r(VO_2)$ fluctuations are characterized by an asymptotic scaling exponent that indicates multifractal anti-persistent or uncorrelated dynamics. For both scaling regimes, a generalization of the multiplicative cascade model provides very good fits for the Renyi exponents $\tau(q)$, showing that the infinite number of exponents $h(q)$ can be described by only two independent parameters, a and b. We also show that the long-range correlation structure of $r(VO_2)$ time series differs from randomly shuffled series, and may not be explained as an artifact of stochastic sampling of a linear frequency spectrum. These results show that metabolic rate dynamics in a well studied micro-endotherm are consistent with a highly non-linear feedback control system.

PeerJ Preprints | https://doi.org/10.7287/peerj.preprints.2404v1 | CC BY 4.0 Open Access | rec: 1 Sep 2016, publ: 1 Sep 2016

Introduction

Physiologic complexity is ubiquitous in all living organisms (West et al. 1994; Glass 2001; Golberger et al. 2002; Burggren & Monticino 2005). It emerges as the result of interactions among multiple structural units and regulatory feedback loops, all of which function over a wide range of temporal and spatial scales, allowing the organism to respond to the stresses and challenges of everyday life (West et al. 1994; Goldberger et al. 2002). As a consequence of these intricate regulation feedbacks, most physiological state variables typically present non-linear, non-stationary dynamics, with irregular fluctuations that follow power-law probability distributions and present long-range correlations over multiple time scales (Glass 2001; Goldberger & West 1987; Kantelhardt 2011; Labra et al. 2007; Mantegna & Stanley 2000; West et al. 1994). The application of analytic techniques from nonlinear dynamics and statistical physics to the study of different physiologic variables has led to the proposition of a general theory to account for the complexity of physiologic variables (Glass 2001; Costa et al. 2002; Goldberger et al. 2002; Kantelhardt 2011; Lipsitz 2004). This theory states that, given certain parameter conditions, the state variables of healthy systems reveal complex variability associated with long-range (fractal) correlations, along with distinct classes of nonlinear interactions (Goldberger 1996; Goldberger et al. 1990; Goldberger et al. 2002). Over the last two decades, different studies have shown that the break down of this type of multi-scale, nonlinear complexity is a characteristic signature of disease and senescence, and as a result, the study of complexity in physiological variables has shown important promise in the efforts to understand and diagnose different pathologies (Costa et al. 2008; Delignières & Torre 2009; Goldberger et al. 2002; Hausdorff et al. 2001; Hu et al. 2004; Ivanov et al. 2007; Lipsitz 2004).

While different quantitative approaches have been devised to measure the degree of complexity in physiological signals (e.g. Burggren & Monticino 2005; Costa et al. 2002; Feldman & Crutchfield 1998; Pincus 1991; Rezek & Roberts 1998; Richman & Moorman 2000; Schaefer et al. 2014), most studies examining changes in physiological complexity as a result of pathological alterations have been conducted by examining either the change or loss of long-range correlations of physiologic signals (e.g. Costa et al. 2008; Delignières & Torre 2009; Goldberger et al. 2002; Hausdorff et al. 2001; Hu et al. 2004; Ivanov et al. 2007; Lipsitz 2004). Long-range correlated time series typically exhibit slowly decaying auto-correlation functions *C(s)* across different time scales *s*, which are characterized by power law decay:

$$C(s) \propto s^{-\gamma} \qquad (1)$$

with scaling exponent taking values in the range $0<\gamma<1$, such that a characteristic correlation time scale cannot be defined (Chaui-Berlinck *et al.*, 2002a; Chaui-Berlinck *et al.*, 2002b; Billat *et al.*, 2006; Kantelhardt 2011). It has been argued that the lack of a characteristic scale in physiological systems may help the organism to be more stable and adaptive to internal and external perturbations by preventing the emergence of periodic behaviors or phase locking, thus avoiding any restriction to the functional responsiveness of the organism in the face of external perturbations (Peng et al. 1993; Peng et al. 2002, West & Shlesinger 1989). If this were correct, the study of long-range correlations would provide important insights on the degree of regulation and homeostasis of living organisms, as well as potential tools in the diagnosis of certain pathologies. A power law scaling of the spectrum of Fourier frequencies may also describe the presence of long-term correlations in any given stationary physiological signal:

$$S(f) \sim f^{-\beta} \quad (2)$$

Long-range correlated processes of this type are often referred to as $1/f^{\beta}$ processes or noises, and are characterized by a unique value of the scaling exponent β, which provides a measure of the type of long-range correlation (Chaui-Berlinck *et al.*, 2002a; Chaui-Berlinck *et al.*, 2002b; Billat *et al.*, 2006; Kantelhardt 2011; Schaefer et al 2014). Again, the power law scaling implies that no single characteristic scale may be identified. The Fourier power spectrum scaling exponent may be related to the correlation function exponent by the relationship $\beta=1-\gamma$. Further, the different scaling exponent values are associated with different types of correlation structure in a given time series or signal. Thus, for processes where $\beta=0$ (or $\gamma=-1$) the signal shows no long-range correlation between values, while values where $\beta>0$ (or $\gamma>-1$) describe a process with long-range correlation or persistence. Processes where $\beta<0$ (or $\gamma<-1$) describe a signal with long-range anti-correlations, or anti-persistence, where large values are followed by small ones (Witt & Malamud 2013). Nevertheless, the use of frequency spectra requires not only that the time series be stationary, but also the use of particular binning procedures as well as averaging over a large number of realizations in order to accurately estimate the value of the scaling exponent β (Kantelhardt 2011; Witt & Malamud 2013). An alternative approach for non-stationary time series is to characterize its long-range persistence by examining the self-affinity of the profile or cumulative sum $z_i = \sum r(VO_2,i)$, for all samples $i=1$ to N (Peng et al. 2002, Kantelhardt 2011). Examination of these time series requires us to take into account that the time axis and the axis of the measured values $x(t)$ are not equivalent quantities, and that a rescaling of time t by a factor a may require rescaling of the series values $x(t)$ by a different factor a^H in order to obtain a signal that is statistically self-similar to the original one (Kantelhardt 2011). Hence, the exact type of

self-affinity or statistical self-similarity in a time series may be described by the resulting scaling relation $x(t) \rightarrow a^H x(at)$ where H corresponds to the Hurst exponent, which measures the degree of persistence or predictability of the profile or cumulated time series (Kantelhardt 2011). The exponent H may be studied by different methods including rescaled range analysis, fluctuation analysis, and detrended fluctuation analysis (Peng et al. 2002, Kantelhardt 2011). In particular, Detrended fluctuation analysis (DFA) has been widely employed to reliably detect long-range autocorrelations in non-stationary time series, with a large number of studies using it to report long-range autocorrelations, although a few studies have reported anti-persistent anti correlations (e.g. Bahar et al. 2001; Delignières et al. 2006, 2011; Kantelhardt 2011). The value of the Hurst exponent H may be approximated by the DFA, which calculates the scaling of mean-square fluctuations with time series scale, yielding the scaling exponent α (Feder 1988; Hurst 1951; Peng et al. 2002, Kantelhardt 2011). When DFA scaling relationships are observed, the scaling exponent $\alpha \approx H$ is related to the correlation exponent γ by the relationship $\alpha = 1 - \gamma/2$, with $\alpha = 0.5$ being the threshold between anti persistence and persistence (Peng et al. 2002, Kantelhardt 2011).

Despite the increased interest to study fractal or long-range correlated dynamics across many systems, in some highly nonlinear complex systems, the resulting time series presents a scaling autocorrelation function and frequency power spectrum which may be better described by a large number of scaling exponents rather than by a single scaling exponent value (Kantelhardt 2011). Thus, one may distinguish between monofractal and multifractal signals. Monofractal signals present a long-range correlation structure where a single scaling exponent suffices to describe the

123 correlation scaling. On the other hand, multifractal signals require an infinite spectrum of scaling
124 exponents to describe their correlation structure (Humeau et al. 2009; Ivanov et al. 1999;
125 Kantelhardt 2011; Suki et al. 2003; West & Scafetta 2003). Thus, multifractal time series are
126 heterogeneous, showing a given value of the self-affinity exponent only in local ranges of the
127 signal structure, such that their self-affinity exponent varies in time. Hence, multifractal signals
128 may be characterized by a set of local fractal sets that represent the support for each Hurst
129 exponent value (Bassingthwaighte et al. 1994; Ivanov et al. 1999; Kantelhardt 2011). In this
130 regard, multifractal time series are more complex than monofractal ones, and determining
131 whether a given complex physiologic system presents monofractal or multifractal dynamics may
132 provide insight on the degree of complexity or nonlinearity of the underlying control
133 mechanisms (Mantegna & Stanley 1997).

134 In endotherms, metabolic rate (VO_2) is a global emergent property that reflects the sum of the
135 energetic costs required to maintain homeostasis, allowing body temperature (*Tb*) to remain as
136 constant as possible despite any changes of its surrounding ambient temperatures (*Ta*) (Karasov
137 & Rio 2007; Lighton 2008; McNab 2002). Under controlled laboratory conditions, it is possible
138 to identify a range of optimal *Ta* values where *Tb* may be kept constant without changes in
139 energy expenditure, but rather as a result of adjustments to physical processes (i.e. conductance,
140 radiation, and convection). Within this range of *Ta* values VO_2 is expected to show minimal
141 variation, and hence it is named the thermo-neutral zone (*TNZ*) (Bozinovic & Rosenmann 1988;
142 Chaui-Berlinck et al. 2005; Karasov & Rio 2007; Lighton 2008; Lipsitz 2004; McNab 2002). A
143 striking characteristic of VO_2 signals is that, even within the *TNZ*, they may be non-stationary,
144 showing changes in the mean and variance of the time series (Chaui-Berlinck et al. 2002a).
145 Studies with small endotherms have shown that VO_2 dynamics within the *TNZ* present irregular

fluctuations with long-range correlations, evidenced by the presence of a single monofractal $1/f^{\beta}$ scaling exponent in the Fourier frequency spectrum (Chaui-Berlinck *et al.*, 2002a; Chaui-Berlinck *et al.*, 2002b; Billat *et al.*, 2006). Thus, within the *TNZ*, VO_2 shows complex dynamics that are consistent with a dynamical system under non-linear control (Chaui-Berlinck et al. 2005). The non-stationary behaviour in metabolic rate may be examined by analysing the rate of change in oxygen consumption, $r(VO_2)$ as a measure of the fluctuations of VO_2. It is defined as $r(VO_2)=log10[VO_2(t+1)/ VO_2(t)]$ (Labra et al. 2007). This variable reveals whether clusters of large, abrupt changes may be seen in the $r(VO_2)$ time series, or if similar variability is observed throughout. In addition, the calculation of $r(VO_2)$ allows the de-trending of the data, yielding a much more stationary time series. Examination of $r(VO_2)$ time series for different species of small mammals, birds and reptiles have shown that this variable has a symmetric power law probability distribution, centered in $r(VO_2)$=0, with a universal triangular shape that does not change across different species (Labra et al. 2007). Thus, metabolic rate fluctuations follow a single statistical distribution despite differences in cardiovascular and respiratory designs, with distribution width scaling inversely with individual body size (Labra et al. 2007). However, to date, the correlation structure in $r(VO_2)$ has not been examined. In a similar fashion to other complex non-linear time series, long-term correlations in $r(VO_2)$ would mean that large fluctuations are more likely to be followed by another large oscillation, while a small oscillation is likely to be followed by a small oscillation (Ashkenazy et al. 2003; Bunde & Lennartz 2012). If this were the case, the expected average value of VO_2 would increase, showing a persistent trend. For VO_2 to show homeostatic regulation however, its fluctuations would be expected to show anti-persistence over at least at some scales, so that large $r(VO_2)$ increases may be followed by large $r(VO_2)$ decreases, ensuring that overall average VO_2 values remain under homeostatic

169 control. Thus, the presence of anti-persistent correlations may be expected for $r(VO_2)$ time series,
170 particularly if there are strong control feedback loops regulating total energy expenditure in an
171 organism. This suggests that examination of the type of autocorrelations present in $r(VO_2)$ time
172 series, as well as the range of time scales involved may provide insight on the regulation
173 feedback that may be acting on metabolic rate at the level of the organism. To gain some
174 understanding of how this may be so, we examine the relationship between thermal stress and
175 VO_2 fluctuations.

176

177 In endotherms, VO_2 fluctuations are expected to be proportional to the environmental thermal
178 challenges, measured as changes in the difference ($Tb - Ta$) (Bozinovic & Rosenmann 1988;
179 Chaui-Berlinck et al. 2005; Karasov & Rio 2007; Lighton 2008). Outside the *TNZ*, adjustments
180 to the body's thermal conductance are not enough to sustain thermal homeostasis, and
181 consequently additional physiological and biochemical process are required in order to keep
182 constant the internal state, which leads to an increase both VO_2 and presumably $r(VO_2)$ as well.
183 In the case of small endotherms, their body size leads to higher challenges associated to the loss
184 of temperature resulting from the large body surface through radiation (Chaui-Berlinck et al.
185 2005; Karasov & Rio 2007; Lighton 2008; Lipsitz 2004; McNab 2002). Given the intricate
186 nature of the network of control processes involved in achieving constant *Tb* (Chaui-Berlinck et
187 al. 2005), it is reasonable to expect that when faced with lower environmental temperatures
188 values below the *TNZ*, endothermic homeostatic processes would be accompanied by a more
189 complex pattern of auto-correlations. To determine whether this is the case, we use fractal and
190 multifractal analysis to examine whether the correlation structure of VO_2 shows any changes as a

191 result of decreasing environmental temperatures. In this regard, a working hypothesis is that for
192 *Ta* values below the *TNZ* the $r(VO_2)$ signal should show a more complex pattern of long-range
193 correlations, resulting in a broader range of autocorrelation scaling exponents, as expected for
194 multifractal signals. These changes should come about as a result of the activation of internal
195 feedback mechanisms to regulate *Tb*. A related question to this prediction concerns the form of
196 this possible relation between complexity and decreasing of *Ta*. Records in wild rodents show a
197 monotonic and linear increment of average VO_2 in animals exposed to *Ta* decreasing (30°C to
198 0°C) (Bozinovic & Rosenmann 1988), suggesting that VO_2 and $r(VO_2)$ complexity levels may
199 also increase linearly. An alternative outcome may be the gradual decrease and eventual loss of
200 complexity, due to a drop in the efficiency of the thermoregulatory feedback control at lower
201 temperatures (Angilletta 2006; McNab 2002). This second pattern would be in agreement with
202 the hypothesis of loss of physiological complexity in the face of extreme system degradation or
203 acute stress (Goldberger et al. 2002). To test these hypotheses we examine the fractal properties
204 of time series of $r(VO_2)$ measurements n laboratory mice (*Mus musculus*) exposed to
205 environmental temperatures ranging from *TNZ* (30ºC in this species) to 0°C. Thus, as first step in
206 this work we assess whether $r(VO_2)$ values exhibit either monofractal or multifractal long-term
207 correlations under different environmental temperatures. We do this by testing whether
208 metabolic rate fluctuations show any long-range correlations, and if so, testing whether there
209 may be described either by a single scaling exponent or if multiple scaling exponents are
210 required, using the multifractal detrended fluctuation analysis (MF-DFA) method. We then
211 assess how these quantitative descriptors of long-range correlations vary with environmental
212 temperature, assessing how they change with decreasing values of *Ta*.

213

Methods

Determination of Metabolic rate

Empirical VO_2 time series were determined by measuring metabolic rate in wild-type male white laboratory mice. Mice were transferred to the laboratory and housed individually with sawdust bedding. Mice were provided with water and fed with food pellets *ad libitum*. Ambient temperature and photoperiod were held constant at 20 ± 2°C and 12L:12D respectively. Care of experimental animals was in accordance with institutional guidelines. The Bioethics commissions of Universidad Santo Tomás, Pontificia Universidad Católica de Chile, and The Chilean National Committee of Science and Technology (CONICYT) approved all experimental protocols followed. Animals were held under these conditions for two weeks prior to measurements and then fasted for 3 h immediately prior to metabolic rate records in metabolic chambers (Lighton 2008). Individuals were measured at seven different *Ta*, 0°C, 5°C, 10°C, 15°C, 20°C, 25°C and 30°C, with the latter corresponding to the lower limit of *TNZ* in this species. Overall, 18 individuals were assigned to different temperature treatments, with the order of temperature treatments for each individual assigned at random to avoid any artefacts. In addition, colonic body temperature (T_b) was recorded at the end of each measurement using a Digi-Sense copper-constant thermocouple to evaluate a possible torpor condition at the end of the experiment. In each experimental record VO_2 was measured in a computerized open-flow respirometry system (Sable Systems, Las Vegas, Nevada). The metabolic chamber received dried air at a rate of 800 ml/min from mass flow-controllers (Sierra Instruments™, Monterey, California), which ensured adequate mixing in the chamber. Air passed through CO_2 and H_2O absorbent granules of Baralyme™ and Drierite™ respectively before and after passing through the chamber and was monitored every 1 sec. This allowed us to obtain time series of oxygen

consumption recorded at periodic intervals of $t=1$ second. After the $r(VO_2)$ time series were registered, they were then analysed by calculating the corresponding $r(VO_2)$ time series.

Assessing long range correlations in metabolic rate

To determine the presence of long-term correlations in the $r(VO_2)$ time series, we examined the power spectral density $S(f) \equiv |x(f)|^2$, where $x(f)$ is the Fourier transform of $r(VO_2)$ data observations measured under experimental conditions (x_i) evaluated at frequencies $f = 0, ..., N/2$ (Bunde & Lennartz 2012; Kantelhardt 2011). As mentioned above, for long-term correlated time series, it can be shown that the power spectral density decays with frequency following a power law (see Equation 2). In order to avoid potential artefacts due to lack of stationary behaviour, we also used the Detrended Fluctuation Analysis method (DFA) (Kantelhardt 2011; Peng et al. 1995a). Briefly, DFA analyses a profile or accumulated data series $z_i = \sum r(VO_2,i)$, for all samples $i=1$ to N. The profile is divided into N_s non-overlapping segments of scale s. For every segment v, the local trend is fit by a polynomial of order n, and the variance raised to the 2-th power $[\sigma^2(v,s)]^2$ between the local trend and the profile in each segment ν is calculated. The mean fluctuation function $F(s)^2$ is then calculated by:

$$F_2(s) = \left\{ \frac{1}{N_s} \sum_{v=1}^{N_s} \left[s^2(s) \right] \right\}^{1/2} \qquad (3)$$

(equation 3: $F_2(s)=[1/N_s][\Sigma(s^2(s))]^{1/2}$)

Examination of how $F_2(s)$ scales with box size or scale s allows the estimation of the scaling

exponent α_{DFA}, which is often referred to as the global Hurst exponent H (Goldberger et al. 2002; Ivanov et al. 2007; Kantelhardt 2011; Peng et al. 1995a). When observed time series are either uncorrelated or show short term correlations, α_{DFA}=0.5 (Kantelhardt 2011; Peng et al. 1995a). For long-term correlated data with persistent $1/f^{\beta}$ noise, where $\beta=1.0$, α_{DFA} exhibits values of equal to 1.0. For values of α_{DFA} below 0.5, the series is said to be anti-persistent, with positive trends being associated with negative trends (Delignières et al. 2006, 2011).

Assessing multifractality of metabolic rate

To determine the presence of multifractality in the fluctuations of metabolic rate we applied multifractal detrended fluctuation analysis (MF-DFA) (Kantelhardt 2011; Kantelhardt et al. 2002) to $r(VO_2)$ data measured under experimental conditions. This method yields similar results to other existing methods of multifractal analysis in time series (Ivanov et al. 2007; Kantelhardt 2011; Kantelhardt et al. 2002; Ludescher et al. 2011; Oswiecimka et al. 2006), but is considerably easier to implement, being based on an extension of DFA (Kantelhardt 2011; Kantelhardt et al. 2002; Ludescher et al. 2011). Briefly, MF-DFA analyses a profile or accumulated data series $z_i = \sum r(VO_2,i)$, for all samples $i=1$ *to* N. The profile is divided into N_s non-overlapping segments of scale s. For every segment v, the local trend is fit by a polynomial of a given order o, where o=1,2 or 3. The resulting variance is then raised to the q/2-th power $[\sigma^2(v,s)]^{q/2}$ between the local trend and the profile in each segment ν is calculated. When $q = 0$, logarithmic averaging may be applied (Kantelhardt 2011; Kantelhardt et al. 2002; Ludescher et al. 2011). A generalized fluctuation function $F_q(s)$ is then calculated by averaging all the variances across all segments of scale s:

$$F_q(s) = \left\{ \frac{1}{N_s} \sum_{v=1}^{N_s} [\sigma^2(v,s)]^{q/2} \right\}^{1/q} \quad (4)$$

(equation 4: $F_q(s)=[1/N_s][\Sigma(\sigma^2(v,s))]^{q/2})^{1/q}$

In general, $F_q(s)$ exhibits a scaling relationship with time scale s: $F_q(s) \sim s^{h(q)}$, which allows the estimation of a set of exponents $h(q)$ for every moment q. These scaling exponents correspond to the generalized Hurst exponents. In some nonlinear complex systems, the $F_q(s)$ function has been shown to exhibit scaling crossovers, with more than one asymptotic scaling exponent (Koscielny-Bunde et al. 2006). Hence, we tested whether linear or piecewise linear regressions best fit the scaling relationship of $F_q(s)$ with s, using log-transformed data. The piecewise or segmented relationship between the mean response $\mu = E[Y]$ and the variable X, for observation $i = 1, 2,...,n$ was modeled by adding the following terms in the linear predictor:

$$\beta_0 + \beta_1 X_i + \beta_2 (X_i - \delta) + \quad (4)$$

where $(X_i - \delta)+ = (X_i - \delta) \times I(X_i > \psi)$, and δ is the fitted breakpoint or crossover point and $I(\cdot)$ is an indicator function that is equal to one when the statement is true and is equal to zero when the statement is false (Muggeo 2003). Piecewise linear models were fitted using the *segmented* library (Muggeo 2003) in the R program (R Development Core Team 2014, available at www.r-project.org). If no crossovers were observed, then linear regression would be favored over a piecewise regression. To test this, the *segmented* library uses Davie's test to test for a non-constant regression parameter in the linear predictor (Muggeo 2003). Once the correct regression model is identified, the regression slopes provide the asymptotic estimates for the scaling exponents $h(q)$. If no crossover is present, only one scaling exponent $h(q)$ is obtained for every

297 moment q. If a crossover point is detected, then two scaling exponents $h(q)$ and $h(q)$ are obtained
298 for every moment q.

299 For monofractal self-affine time series, $h(q)$ is independent of the chosen moment q, and
300 is identical to the global Hurst exponent H regardless of the value of the moment q (Feder 1988;
301 Hurst 1951; Kantelhardt et al. 2003; Kantelhardt et al. 2002). Hence, for monofractal self-affine
302 time series $\alpha_{DFA} \approx H$. On the other hand, in multifractal time series $h(q)$ varies with q, reflecting
303 the fact that small and large fluctuations scale differently (Kantelhardt et al. 2002). For negative
304 values of q, $h(q)$ describes the scaling behaviour of those time series segments with small
305 fluctuations, whereas for positive values of q, $h(q)$ describes the scaling behaviour of those time
306 series segments with large fluctuations (Kantelhardt et al. 2002). It has been shown that the
307 generalized Hurst exponent $h(q)$ can be directly related to the classical multifractal scaling Renyi
308 exponents $\tau(q)$ defined by the standard partition function-based formalism using the
309 relationships: $\tau(q) = qh(q) - 1$ and $h(q) = (\tau(q)+1)/q$ (Kantelhardt et al. 2002; Koscielny-
310 Bunde et al. 2006). Thus, it may be shown for normalized, stationary time series that the
311 multifractal spectra estimated by MF-DFA have a deep similarity with thermodynamics
312 (Kantelhardt et al. 2002).

313 For monofractal records, $\tau(q)$ is a linear function of q, while multifractal records are
314 characterized by non-linear dependence of $\tau(q)$ on q (Ivanov et al. 1999; Kantelhardt et al. 2002;
315 Koscielny-Bunde et al. 2006). Also, it can be shown that $h(q)$ may be related to the singularity
316 spectrum $f(\alpha)$ via a Legendre transform:

317 $$f(\alpha) = q[\alpha - h(q)] + 1 \qquad (5)$$

where $\alpha = [d\tau (q)/dq]$ is the singularity strength, or Hölder exponent, while $f(\alpha)$ denotes the singularity dimension of the subset of the time series that is characterized by a given value of singularity strength α (Feder 1988; Kantelhardt et al. 2002; Ludescher et al. 2011, Ihlen 2012). For monofractal self affine signals, the singularity spectrum of the time series is a single point, showing that there is a unique value or a very small set of values of singularity strength α, with a corresponding fractal dimension $f(\alpha) = 1$. For multifractal self affine signals, the singularity spectrum of the time series is a parabola, with a maximum at the dominant singularity strength observed in the time series.

To assess multifractality in $r(VO_2)$ time series, we calculated the fluctuation function $F_q(s)$ for data obtained from wild-type white laboratory mice $r(VO_2)$ time series measured under controlled conditions. Following recent studies, we fit both the $h(q)$ and $\tau(q)$ spectra with a modified version of the multiplicative cascade model, which has been proposed by (Koscielny-Bunde et al. 2006):

$$h(q)=(1/q) - (\ln(a^q+b^q))/(q\ln(2)) \quad (6)$$

and

$$\tau(q)=-(\ln(a^q+b^q))/(\ln(2)) \quad (7)$$

The modified multiplicative cascade model functions (MMCM) allows the description of multifractal spectra with only two parameters, a and b, which take values between 0 and 1 with $a + b \geq 1$. An additional advantage is that these functions also extend to negative q values, and thus allow estimation of the multifractal spectrum $f(\alpha)$ for these values as well (Koscielny-Bunde et al. 2006). Using the $\tau(q)$ spectra, we estimated the parameters a and b for eqn. (7), allowing us

to obtain continuous $\tau(q)$ and $f(\alpha)$ spectra from the MMCM fits.

To test whether observed long term correlation behaviour was different from a random expectation, we randomized all time series using an amplitude-adjusted Fourier transform algorithm (AAFT) (Schreiber & Schmitz 1996; Schreiber & Schmitz 2000). The scaling functions were calculated for all surrogate time series and the corresponding scaling exponents (e.g. β and α_{DFA} for Fourier spectral density and DFA respectively) were calculated (Schreiber & Schmitz 1996; Schreiber & Schmitz 2000).

Assessing the effect of temperature on multifractality of metabolic rate fluctuations

As explained above, regular VO_2 time series were obtained under temperature-controlled conditions (see Methods sections for details). To assess the effect of Ta on long range and multifractal measures of $r(VO_2)$ fluctuations, we calculated the average fluctuation function $F_q(s)$ for each of the seven temperature treatment groups, testing whether the resulting $h(q)$ and $\tau(q)$ spectra are also multifractal. In order to summarize the observed results, we calculated the singularity spectrum $f(\alpha)$, which allows a compact description of the degree of multifractality through the quantification of $\Delta\alpha$, the width of the singularity spectrum as well as the average dominant exponent α_{max} , which indicates which is the dominant scaling exponent, or the one which shows greater support on average across the time series. We then summarized the various spectra across the experimental temperature treatments, allowing us to examine their response to temperature. To test whether observed multifractal behaviour was different from a random expectation, we randomized all time series using an amplitude-adjusted Fourier transform algorithm (AAFT) (Schreiber & Schmitz 1996; Schreiber & Schmitz 2000). After the surrogates were generated, the general fluctuation function $F_q(s)$ and the $h(q)$ spectra were calculated as

361 explained above. We then compared *h(q)*, *τ(q)* and *f(α)* spectra for the shuffled time series.
362 Again, we summarized the various spectra for shuffled time series across the experimental
363 temperature treatments, allowing us to compare them with original time series spectra as for
364 different temperature treatments. To assess the potential effect of de-trending polynomial order
365 *o,* all data analyses were carried out for each individual time series were carried out using three
366 orders: *o*=1, 2 or 3. Data analyses were carried out using Matlab R2011b and R software (R
367 Development Core Team 2014, available at www.r-project.org).

368

369

370 **Results**

371 As described in the physiological literature for endotherms, average VO_2 values in the lab mouse
372 show a marked thermal response below *TNZ,* with higher VO_2 values that increase away from
373 basal metabolic rate (*BMR)* as *Ta* becomes progressively lower (Figure 1a). None of the animals
374 studied showed signs of torpor either during or after the VO_2 measurements, and observed *Tb*
375 varied from 36.0 to 37.3 ºC across all records. However, even within the *TNZ* (30°C), typical
376 VO_2 time series exhibit irregular non-stationary fluctuations (Figure 1b). The rate of change
377 $r(VO_2)$ yields a de-trended time series, which reveals abrupt changes in VO_2 , with clusters of
378 large fluctuations separated from clusters of smaller fluctuations(Figure 1c). This suggests the
379 presence of long-term correlation or persistence in these time series. The clustering of large
380 fluctuations is lost when data are shuffled randomly using AAFT (Figure 1d), providing
381 indication that the observed pattern of $r(VO_2)$ fluctuations may be associated with the
382 autocorrelation structure of the time series (Schreiber & Schmitz 1996; Schreiber & Schmitz

2000; Kantelhardt 2011) rather than with the fat tailed probability distribution shown by this variable (Labra et al. 2007). The statistical pattern of autocorrelation in the sequence of large and small fluctuations may be examined by calculating the Fourier frequency power spectra, which reveals the presence of long-term correlations, shown by a 1/f-like scaling exponent (Figure 1e). On the other hand, shuffled time series exhibit a shallower power spectrum, indicating the loss of these long-term correlations (Figure 1e) (Kantelhardt et al. 2002; Schreiber & Schmitz 1996; Schreiber & Schmitz 2000). However, while $r(VO_2)$ time series do not exhibit obvious trends in the mean, they do show changes in variability through time, and as a result may not meet the statistical assumptions of spectral frequency estimation (Kantelhardt 2011). Examination of detrended fluctuation analysis reveals a scaling crossover, with two clear scaling regimes shown by the root mean square fluctuation function $F_2(s)$ (Figure 1f). This suggests that a single scaling exponent may not be sufficient to characterize the autocorrelation of $r(VO_2)$ fluctuations (Kantelhardt et al. 2002). In this time series, the scaling exponent for small time scales (s <100 seconds), α_{DFA1}, indicates the presence of persistent, long-range correlated fluctuations (α_{DFA1}=0.91) (Figure 1f). However, for larger time scales (s>100 seconds) we see that fluctuations over these time scales are anti-persistent, with the second scaling exponent α_{DFA2}=0.39 (Eke 2000, Delignières et al. 2006, 2011). As mentioned above, in anti-persistent time series dynamics positive trends are usually followed by negative trends, thus showing a phenomenological signature of control or negative feedback over the rate of change of VO_2 (Delignières et al. 2011). Shuffling the data results in a loss of the observed crossover scaling behaviour, indicating this is property is not a result of randomness in the pattern of fluctuations (Figure 1f). Thus, we find that $r(VO_2)$ fluctuations within the TNZ show non-trivial long-range correlations, in agreement with previous observations for VO_2 in small endotherms (Chaui-

406 Berlinck *et al.*, 2002a, 2002b). However, a single scaling exponent does not suffice to describe
407 these long-range correlations.

408

409 When we examined the DFA scaling functions for $r(VO_2)$ fluctuations both within and
410 outside the *TNZ*, we observe a similar crossover pattern across different temperatures, with
411 average $F_2(s)$ scaling functions show a crossover pattern which is similar to that observed in
412 Figure 1f. Hence, observed scaling exponent values for small to intermediate time scales) are
413 consistent with persistent long-range autocorrelations (i.e. $0.5<\alpha_{DFA1}<1.0$) (Figures 2a to 2d). On
414 the other hand, for intermediate to large scales, the scaling exponent values are consistent with
415 anti-persistent long-range correlations ($\alpha_{DFA2}<0.5$) (Figures 2a to 2d). Shuffling the individual
416 time series results in changes to the $F_2(s)$ scaling functions, with average α_{DFA1} values becoming
417 smaller (Figures 2e to 2h). Examination of the scaling exponent values shows that α_{DFA2} values
418 do not show large changes for shuffled data (Figure 3). This pattern is observed for linear (Figure
419 3) as well as for quadratic and cubic de-trending orders *o* (see Supplementary Figure 1). The
420 existence of two scaling regimes for the long-range correlations of $r(VO_2)$ may be interpreted as
421 evidence that two dominant scaling exponents may suffice to account for the correlation
422 structure of the $r(VO_2)$ time series. An alternative possibility may be that a continuous spectrum
423 of scaling exponents are required in order to account for the observed pattern of long-term
424 correlations in VO_2 fluctuations. If the latter were the case, local scaling exponents would show a
425 large number of possible values.

426 To visualize whether a sample $r(VO_2)$ time series is consistent with a multifractal process,
427 we examined the changes in the value of local DFA scaling exponent α_{DFA} through time in the

time series shown in Figure 1 (which was measured within the TNZ). We calculated the local value of α_{DFA} as for a moving window placed along the time series. We calculated α_{DFA} values using moving windows of 128, 256 and 512 seconds (Figures 4a, 4b and 4c respectively). All these window sizes correspond to the asymptotic exponent expected for the second scaling regime identified before for this time series (Figure 1f). Observed local α_{DFA} exponent values change through time for all window sizes used, forming an irregular pattern (Figure 4). Further, α_{DFA} values range broadly between 0.5 and 1.5, as shown by the blue lines in Figure 4. Thus, while in some sections show exponent values close to 1.0, corresponding to persistent power law long-range correlations, other sections may show values closer to either 1.5 (corresponding to persistent Brownian motion) or to 0.5 (corresponding to uncorrelated fluctuations) (Peng et al. 1995b). There are also sections where the local α_{DFA} scaling exponent may take values below 0.5, corresponding to anti-persistent fluctuations (Eke 2000, Delignières et al. 2006, 2011). Again, random shuffling of the time series destroys the observed pattern of irregular fluctuations of α_{DFA}, with all exponent values clustering around 0.5, as shown by the red lines in Figure 4. Thus, for this time series, we can see that observed $r(VO_2)$ fluctuations cannot be characterized by a single scaling exponent, and hence may be multifractal.

To determine whether this is the case, we examined whether the MF-DFA formalism can describe VO_2 fluctuations across different environmental temperatures. Figure 5 shows the average MF-DFA generalized fluctuation functions $F_q(s)$ calculated from time series measured at 30°, 20°, 10° and 0°C (Figures 5a, 5b, 5c and 5d respectively). Across all temperatures studied, and for all the values of q examined, observed $F_q(s)$ functions show a crossover δ that defines two scaling regions, as shown by the fitted piecewise linear regressions (shown in black lines) (Figure 5). Shuffling the time series leads to some changes in the crossover pattern, although no

striking overall pattern may be discerned by qualitative examination (Figures 5e to 5f). It must be noted that while the remaining three series for 5°, 15° and 25°C are not shown, they show similar patterns. In fact, detailed examination of the average generalized fluctuation functions reveals that $F_q(s)$ show the presence of crossover time scales δ for all temperatures studied, regardless of the order *o* of the de-trending polynomial used (see supplementary Figures 2 to 8 for detailed results for different de-trending polynomial orders and all temperatures from 0ºC to 30ºC). Thus, for all temperatures examined, regardless of the order of de-trending polynomial used, we observed two scaling regimes are present, with the piecewise break point changing as a function of *q* in some cases (see supplementary Figure 9). While it could be argued that such scaling crossovers may be the result of trends associated with non-stationary dynamics in the data, examination of the Augmented Dickey-Fuller Test (ADF test) for all $r(VO_2)$ time series rejected the hypothesis of the presence of trends, and we observed that the ADF test yields $p<0.01$ in all time series. Shuffling of the observed $r(VO_2)$ time series does not completely remove the crossover scales δ or the two observed regimes, but does seem to change the scaling exponent for the first scaling regime (see supplementary Figures 2 to 8). Given the presence of two scaling regimes across all time series studied, we then examined the scaling slopes of the curves for both of these scaling regimes and their change with the exponents *q*. This allowed us to estimate the average Hurst ($h(q)$) and Renyi ($\tau(q)$) spectra for each of these two scaling regimes. We then also fitted the MMCM model to the observed Renyi ($\tau(q)$) spectra, and estimated the singularity spectra ($f(\alpha)$) based on these parameter fits.

When we examined average Hurst ($h(q)$) and Renyi ($\tau(q)$) spectra, as well as the corresponding singularity spectra ($f(\alpha)$) estimated from the MMCM fits on $\tau(q)$, we found that the two scaling regimes differ in their multifractal spectra across the seven temperatures studied.

The left hand column of Figure 6 shows the multifractality of $r(VO_2)$ fluctuations, as indicated by the dependence of $h(q)$ on q for different temperature values. We find that fluctuations of different magnitudes in $r(VO_2)$ time series show different scaling behaviour, similar to what has been observed other complex systems (Bunde & Lennartz 2012; Kantelhardt et al. 2006; Kantelhardt et al. 2002). However, the first and second scaling regimes differ in their behaviour, with smaller time scales (in the approximate range $8 \leq s \leq 100$) showing generalized Hurst exponent $h_1(q)$ values closer to 1.5, while larger time scales (in the approximate range $100 \leq s \leq 1024$) show generalized Hurst exponents decreasing from $h_2(q) \approx 0.9$ to $h_2(q) \approx 0.25$ as the exponent order q increases (Figure 6). Hence, fluctuations on the first scaling regime show long-range correlations or persistence, similar to that of Brownian motion, regardless of the magnitude of the fluctuation. On the other hand, for the second scaling regime, small VO_2 fluctuations are characterized by larger scaling exponents $h_2(q)$, corresponding to power law, long-range correlated persistent dynamics, while larger VO_2 fluctuations present smaller $h_2(q)$ exponent values, corresponding to anti-persistent dynamics (see left hand column in Figure 6). Thus, over intermediate to large time scales, large positive $r(VO_2)$ values are balanced by large negative values. On the other hand, for this range of scales, small $r(VO_2)$ values are persistent, such that small positive increases are followed by similarly valued changes, resulting in gradual positive trends in VO_2. A similar pattern occurs for negative rates of change, which leads to gradual negative trends in VO_2. Shuffling the $r(VO_2)$ time series results in markedly lower values of $h(q)$ scaling exponents for the first scaling regime, indicating the observed, persistent long-range correlation cannot be accounted for by a random sample of the observed spectral density function. On the other hand, in the second scaling regime, a complex response is observed, where shuffling results in changes only for negative and small positive q values, whereas

observed exponents for large positive q values overlap with the exponents from shuffled time series. In fact, with the exception of 30ºC, very large fluctuations in *r(VO2)* do not differ from the random expectation (Figure 6).

Observed differences in the range of *h(q)* exponents for the two scaling regimes can also be observed when examining the Renyi exponent spectra. We observed mostly linear Renyi exponent spectra in the first scaling regime, while the second scaling regime shows nonlinear Renyi exponent spectra as expected for multifractal time series (Kantelhardt 2011) (see central column, Figure 6). This suggests that the first scaling regime should either be monofractal or weakly multifractal, requiring a smaller range of scaling exponents to account for the observed singularities. On the other hand, the second scaling regime is characterized by strong multifractality, with a broader range of scaling exponent values. As observed in previous results, shuffling destroys the observed scaling spectra, with the exception of $\tau(q)$ values observed for positive q , which do not differ from the shuffled spectra (Figure 6). In all the time series we examined, the observed Renyi exponent spectra were fit extremely well my the MMCM model shown in equation 6, with R^2 values for the nonlinear fitting procedure being close to 1.0 in all cases (see Supplementary Figure 10). This allowed us to use the fitted $\tau(q)$ values to estimate the singularity spectra $f(\alpha)$ for each individual, which were then averaged across all the different temperature treatments.

Examination of the average singularity spectra $f(\alpha)$ for different temperature treatments shows that the first scaling regime of these *r(VO2)* time series are monofractal or weakly multifractal, as evidenced by either a single point or a narrower parabola in the (α , $f(\alpha)$) plane (see dashed lines in graphs on the right hand column in Figure 6). These qualitative patterns do not change

519 when quadratic or cubic de-trending polynomials are used (see right hand columns of
520 Supplementary Figures 11 and 12). Indeed, the average degree of multifractality, $\Delta\alpha$ shows that
521 the first scaling regime the strength of multifractality decreases with temperature (see Figure 7).
522 While a similar qualitative pattern is observed for all de-trending polynomial orders, a the
523 decrease with temperature is significant only for the linear de-trending case (linear OLS
524 regression, F=8.202, d.f.=(1,5), p=0.035) (Figures 7a 7b and 7c). In sharp contrast, the second
525 scaling regime shows broad singularity spectra, indicating a much larger degree of
526 multifractality, $\Delta\alpha$ (see continuous lines in graphs on the right hand column in Figure 6). For this
527 second scaling regime, no significant linear trends with temperature were observed, with the
528 exception of the cubic de-trended data (linear OLS regression, F=13.43, d.f.=(1,5), p=0.015)
529 (Figure 7c). Shuffled data tend to show similar degrees of multifractality across different
530 temperatures and orders of detrending polynomials (Figure 7d to 7f).

531 On the other hand, when we examine the exponent α_{max} of the singularity spectra, we see that
532 the first scaling regime is characterized by much stronger singularities, with α_{max} taking values
533 closer to 1.5, being slightly larger for 15ºC and 20ºC (Figures 6i and 6o). On the other hand, the
534 second scaling regime is characterized by weaker stronger singularities, showing values of α_{max}
535 below 0.5 (see right hand column of Figure 6 and Figure 8). Examination of the changes in α_{max}
536 as a function of temperature for the first scaling regime indicates that the value of α_{max} has
537 significant increases with temperature only for the linear and cubic cases (linear de-trending:
538 F=7.52, d.f.=(1,5), p=0.04; cubic de-trending: F=7.52, d.f.=(1,5), p=0.04) (Figure 8a to 8c). In
539 the case of quadratic de-trending, temperature values equal or greater than 15ºC show high
540 values of α_{max}, coherent with the persistent, Brownian motion-like values of $h(q)$ observed
541 before. On the other hand, for the second scaling regime, α_{max} does not show significant changes

with temperature for any de-trending order (Figure 8a to 8c). Shuffled data tend to show similar degrees of multifractality for different temperatures and orders of de trending polynomials, with shuffled data for the first scaling regime clustering around values close to α_{max} =0.9, and shuffled data for the second scaling regime clustering around values close to α_{max} =0.3 (Figure 8d to 8f). Thus, both the observed degree of multifractality $\Delta\alpha$, and the dominant multifractal singularity exponent α_{max} in these two scaling regimes cannot be attributed to random fluctuations.

Discussion

Physiological systems, and their state variables and signals, have been recognized as complex (Burggren & Monticino 2005; Glass 2001). To date, most studies examining the causes and functional implications of the loss of complexity in organisms have largely focused on human biomedicine, aiming to understand either pathologies or the senescence process (Costa et al. 2008; Delignières & Torre 2009; Goldberger et al. 2002; Hausdorff et al. 2001; Lipsitz 2004). In this regard, our study aims to provide a better understanding of the role of physiological complexity in the homeostatic response to thermal challenges, particularly in the context of a changing world climate. Here, we analyzed the dynamics of metabolic rate fluctuations, $r(VO_2)$,under different *Ta's* using a well-studied model organism, the lab mouse *Mus musculus*. Using MF-DFA, our results show that within the *TNZ*, $r(VO_2)$ time series show two distinct scaling regimes in the fluctuation functions $F_q(s)$, with a crossover time scale δ of approximately 10^2 seconds. Examination of the generalized *Hurst* exponents shows that these two scaling regimes correspond to persistent and anti-persistent dynamics for scales below and above the crossover time scale, with the strength of multifractality differing between these two regimes.

When environmental temperature T_a is decreased below the *TNZ*, the observed pattern of multifractal, anti-persistent long-range correlations over longer time scales does not vary a great deal. On the other hand, over short scales, the persistent long-range correlations transition from a weakly multifractal to a monofractal distribution. We now discuss these results

The first aspect we discuss is the robustness of the rather complex long-correlation structure observed for our data. While previous analysis of VO_2 have reported long-range persistent $1/f^{\beta}$ fluctuations, described by a single dominant monofractal scaling exponent (Chaui-Berlinck et al. 2002a; Chaui-Berlinck et al. 2002b), we show here that that VO_2 fluctuations of different magnitudes are clustered throughout the experimental time series with varying types of long-range correlation, depending on the time scale analyzed. Thus, $r(VO_2)$ is a multifractal self-affine signal. This suggests that the feedback control mechanisms underlying rapid changes in energy consumption involve strongly non-linear dynamic processes. Both the observed multifractal exponent spectra and the scaling crossover differ from those observed under a random linear transformation in the frequency domain (Kantelhardt 2011; Schreiber & Schmitz 1996; Schreiber & Schmitz 2000). This indicates that the observed multifractality of $r(VO_2)$ is a robust property of metabolic rate. The existence of this long-range correlation structure indicates the potential for plastic dynamic responses to thermal stress (Goldberger et al. 2002; Ivanov et al. 2007). In this regard, the existence of a crossover, with two characteristic long-range correlation signatures may be related to the dynamics of both VO_2 and $r(VO_2)$. As we have shown for data within the *TNZ* (see Figure 1), VO_2 time series may show periods of higher energy consumption interspersed with periods of lower energy use (Figure 1b). These periods present particularly

586 different patterns of VO_2 changes, which are reflected in the pattern of $r(VO_2)$ fluctuations. Thus,
587 higher average energy uses (larger mean VO_2 values) are associated with less variable values of
588 $r(VO_2)$, in agreement with observed results for inter-specific scaling of $r(VO_2)$ across different
589 vertebrate species (Labra et al. 2007), as well as in diverse complex systems (see references in
590 Labra et al. 2007). Examination of $r(VO_2)$ data using different approaches Fourier power spectra,
591 DFA and MFDFA reveal that small-scale and larger scales present different scaling
592 relationships. The first two methods agree qualitatively with the pattern shown by the MF-DFA
593 $F_q(s)$ fluctuation functions. It is important point to out that that in all series, the scaling crossover
594 was observed regardless of the de-trending polynomial order used in MF-DFA. On the other
595 hand, the type of long-range correlation structure identified was also robust. When data were
596 analysed using MF-DFA using 2nd and 3rd order de-trending polynomials, the scaling regime for
597 smaller time scales is observed to be either weakly multifractal or monofractal across most
598 temperatures, while the second scaling regime is found to be multifractal for all three de-trending
599 orders used in MF-DFA. For the second scaling regime, corresponding to larger time scales, the
600 broadest singularity spectra are observed for 15ºC and 20ºC, with either $\alpha_{max} \approx 0.5$ for first de-
601 trending order MF-DFA, or $0.5 > \alpha_{max} > 1.0$ for 2nd and 3rd de-trending order MF-DFA.

602

603 The second aspect we discuss is the possible explanations for the qualitative changes
604 observed in the long-range correlation structure in the vicinity of 15ºC, as well as their potential
605 significance. Metabolic rate changes are central for the control of *Tb* in endotherms (Chaui-
606 Berlinck et al. 2005; Karasov & Rio 2007). Thus, body temperature in these organisms is
607 regulated through a complex set of processes and feedback relationships involving behavioral,

endocrine, vasomotor and neural processes (Chaui-Berlinck et al. 2005; Karasov & Rio 2007). A recent review on the thermal physiology of *Mus musculus* shows that in this species the lower limit of normothermia ranges between 5 and 15°C (Gordon 2012). Below these temperatures, thermal homeostasis requires increased VO_2, which become nearly twice the BMR. These additional homeostatic requirements may be offset with different thermoregulation strategies that include behavioral, postural and physiological adjustments, all of which carry with them increased energetic costs. Over longer periods of time, these energetic requirements may not be met without resorting to alternative physiological strategies such as torpor (Gordon 2012). Interestingly, individuals in our measurements did not reach the torpor stage, resorting only to individual huddling within the measurement chamber. Studies on thermoregulatory behavior have shown that small mammals such as lab mice form groups by huddling together as a behavioral thermoregulatory response to temperature challenges (Canals et al. 1997; Canals et al. 1998). Interestingly, this behavioral response behaves as a system with a continuous (second-order) phase transition, with a critical environmental temperature value found between 16ºC and 20ºC (Canals & Bozinovic 2011). For low temperatures, individuals spontaneously aggregate, forming groups with a higher fractal dimension and a lower mass-specific metabolic rate. This change in behavior occurs in the same temperature range where we have observed maximal values for the degree of multifractality, supporting the idea that different physiological regimes may occur above and below this temperature range. Hence, future work could examine the long-range correlation properties of VO_2 fluctuations under different strategies such as torpor or group huddling, in order to determine whether the degree of multifractality decreases below that observed at 0°C, giving rise either to monofractal scaling or to the loss of fractal autocorrelations.

631 A third point we discuss is the biological significance of these results. As mentioned earlier,
632 whole-body metabolic rate is an emergent phenomenon, resulting from microscopic interactions
633 with a large number of degrees of freedom and a complex set of opposing feedback mechanisms
634 acting at different time scales (Bozinovic 1992; Chaui-Berlinck et al. 2005). In this regard, the
635 multifractal nature of metabolic rate highlights the complex and non-linear nature of the multiple
636 feedback loops involved in the maintenance of physiological homeostasis (Chaui-Berlinck et al.
637 2005; Darveau et al. 2002; Hochachka et al. 2003). The existence of multifractality in metabolic
638 rate fluctuations has several interesting implications, particularly regarding the sensitivity to
639 initial conditions. In general, multifractal dynamics are generated by non-linear recursive
640 processes, which show different scaling or fractal properties depending on the initial conditions
641 or on the particular history of external disturbances to the system (Kantelhardt 2011). As a result,
642 the observed singularities and scaling exponents of multifractal time series can change in time,
643 leading to the presence of local abrupt shifts in the dynamics of these systems (Kantelhardt
644 2011). In addition, these singularities are associated with the presence of both extreme events
645 and fat tailed power law distributions, which have been shown to be a universal feature of
646 metabolic rate across different vertebrate species (Labra et al. 2007). Despite the seemingly
647 irregular unpredictable nature of metabolic rate fluctuations, our results show that they have a
648 characteristic long-range correlation structure. Although in many applications the proximal
649 mechanistic causes of observed fractality or multifractality have not been elucidated (Kantelhardt
650 2011), the fact remains that multifractal processes such as $r(VO_2)$ are completely different from
651 simple linear random fluctuations. This opens an interesting scenario regarding the potential use
652 of multifractal properties as either a diagnostic tool or as baseline to determine animal response
653 to environmental stress. This improved characterization may also eventually allow the modeling

654 the dynamics and projection of the likelihood of extreme events or prediction of future behavior
655 (Kantelhardt 2011). This may complement the empirical estimates of metabolic rate, which
656 typically correspond to the average value of VO_2 registered in a small section of the time series
657 under specific environmental conditions (Lighton 2008). Similarly, measurements of the rate of
658 VO_2 under the maximum sustainable rate of exercise (i.e. maximal metabolic rate) have been
659 shown to be mostly a function of aerobic capacity of the muscle mass (Weibel et al. 2004). In the
660 light of our results, it seems reasonable to expect that VO_2 fluctuations under conditions of
661 maximum sustainable exercise would also show multifractal long-term correlations as well as
662 power law distributed fluctuations.

663

664 In addition to the physiological significance of long-range multifractal correlations of $r(VO_2)$,
665 a related aspect pertains the taxonomic and systemic generality and significance of our results. It
666 is relevant to discuss whether these observed patterns are expected to hold true for all
667 endothermic species. While previous work on $r(VO_2)$ has reported a universal probability
668 distribution function across different vertebrate species (Labra et al. 2007), no systematic
669 comparative assessment has been carried out to determine if the long-range correlation structure
670 may hold true for different endothermic species, be these birds or mammals. A particularly
671 interesting aspect of such comparisons would be to examine the role of individual body size. Our
672 work was carried out using a small endothermic species, the lab mouse. Analysis of a theoretical
673 model of body temperature control by shifts in metabolic rate has suggested that the rate of heat
674 loss and the capacity to rapidly increase metabolic output may lead to non-equilibrium between
675 metabolic rate and body temperature in micro-endotherms (such as hummingbirds and small

mice), resulting in non-random $1/f^{\beta}$ persistent oscillations of VO_2, even within the *TNZ* (Chaui-Berlinck et al. 2002a). Our results indicate that VO_2 are not only long-range correlated, but that have a complex multifractal structure, which indicates that the model of Chaui-Berlinck et al. (2002a) yields predictions that are at least qualitatively correct. Interestingly, this theoretical model also predicts that larger endotherms such as the rat may not exhibit similar complex oscillations, due to a dynamic equilibrium between metabolic rate and body temperature, given the smaller surface area-volume ratio. If correct, this model predicts the absence of long-range correlated $r(VO_2)$ oscillations for larger endotherms, with multifractal dynamics being found only in micro-endotherms, regardless of whether they are mammals or birds. Whether a threshold body size may be identified below which multifractality may be observed would indicate the onset of a highly nonlinear configuration of control processes acting in the regulation of body temperature. The alternative outcome would be that multifractal long-range correlations also hold true for larger endotherms. This alternative scenario would indicate that a more detailed model analysis is required to account for the processes affecting metabolic rate oscillations.

General Conclusion

While an increasing number of authors have pointed out the complex nature of physiological processes (Burggren & Monticino 2005; Spicer & Gaston 2009), an emerging research question is what are the consequences and implications of physiological complexity for the homeostatic adaptive capability of animals, particularly on a scenario of global climate change. In addition to considering the potential role of organism body size, it is important to determine whether the observed multifractal correlation structure is a general trait of all endotherm taxa, or if it is a

characteristic trait of mammals as a lineage. Comparative experimental studies may help to untangle the relative importance of body size and taxonomic inertia in the emergence of multifractality. A related question is whether ectotherms do present any long-range correlation structure in their metabolic rate dynamics. If complexity is an emergent characteristic arising from the different thermal control feedback loops, then multifractality should be absent in metabolic rate dynamics of reptiles or amphibians. The goal of such studies would be to allow the assessment of the relative importance of universal emergent statistical behaviour and phylogenetic inertia in morphological and physiological traits that may give rise to complex metabolic rate fluctuations. Again, the use of a comparative, controlled experimental approach may allow careful examination of the relationships between the complexity of metabolic rate dynamics and the origins of endothermy.

Our results show that the dynamic response of the metabolic machinery in a model mammal species facing thermal challenge do not reduce themselves to the linear variance response expected , evidencing in addition that this response is regulated by environmental history experienced of individual. In this regards, the humped shape observed from the relationship between complexity level of VO_2 and decrease of temperature agree with a limit at the physiological capability to control of body temperature. Future work in this area may focus on

719 experimental explorations of the physiological basis of long-term correlations and multifractality
720 of VO_2 fluctuations. For example, such work may examine the relative importance of different
721 control mechanisms regulating the rate of oxygen uptake as part of a hierarchical cascade of
722 feedback loops that lead to multifractality.

723

724 **Acknowledgments**

725 We thank F. Boher and S. Clavijo for their assistance during the development of these
726 experiments. FAL thanks C. Huerta and E. Labra for their continued support.

727

728

729 **References**

730 Angilletta MJ. 2006. Estimating and comparing thermal performance curves. *Journal of Thermal*
731 *Biology* 31:541-545.

732 Ashkenazy Y, Baker DR, Gildor H, and Havlin S. 2003. Nonlinearity and multifractality of
733 climate change in the past 420,000 years. *Geophys Res Lett* 30:2146.
734 10.1029/2003gl018099

735 Bassingthwaighte, J. B., & Raymond, G. M. (1994). Evaluating rescaled range analysis for time
736 series. Annals of biomedical engineering, 22(4), 432-444.

737 Bahar, S., Kantelhardt, J. W., Neiman, A., Rego, H. H. A., Russell, D. F., Wilkens, L., ... &
738 Moss, F. (2001). Long-range temporal anti-correlations in paddlefish electroreceptors.
739 EPL (Europhysics Letters), 56(3), 454.

740 Billat, V. L., Wesfreid, E., Kapfer, C., Koralsztein, J. P., & Meyer, Y. (2006). Nonlinear
741 dynamics of heart rate and oxygen uptake in exhaustive 10,000 m runs: influence of
742 constant vs. freely paced. The Journal of Physiological Sciences, 56(1), 103-111.

743 Bozinovic F. 1992. Scaling of basal and maximum metabolic rate in rodents and the aerobic
744 capacity model for the evolution of endothermy. *Physiological Zoology* 65:921-932.

745 Bozinovic F, and Rosenmann M. 1988. Comparative energetics of South American cricetid
746 rodents. *Comparative Biochemistry and Physiology Part A, Physiology* 91:195-202.

747 Bunde A, and Lennartz S. 2012. Long-term correlations in earth sciences. *Acta Geophysica*

748 60:562-588.

749 Burggren WW, and Monticino AG. 2005. Assessing physiological complexity. *Journal of*
750 *Experimental Biology* 208:3221-3232. 10.1242/jeb.01762

751 Canals M, and Bozinovic F. 2011. Huddling Behavior as Critical Phase Transition Triggered by
752 Low Temperatures. *Complexity* 17:35-43. 10.1002/cplx.20370

753 Canals M, Rosenmann M, and Bozinovic F. 1997. Geometrical aspects of the energetic
754 effectiveness of huddling in small mammals. *Acta Theriologica* 42:321-328.

755 Canals M, Rosenmann M, Novoa FF, and Bozinovic F. 1998. Modulating factors of the energetic
756 effectiveness of huddling in small mammals. *Acta Theriologica* 43:337-348.

757 Chaui-Berlinck JG, Bicudo J, Monteiro LHA, and Navas CA. 2002a. Oscillatory pattern in
758 oxygen consumption of hummingbirds. *Journal of Thermal Biology* 27:371-379. Pii
759 s0306-4565(02)00005-010.1016/s0306-4565(02)00005-0

760 Chaui-Berlinck JG, Monteiro LHA, Navas CA, and Bicudo J. 2002b. Temperature effects on
761 energy metabolism: a dynamic system analysis. *Proceedings of the Royal Society B:*
762 *Biological Sciences* 269:15-19. 10.1098/rspb.2001.1845

763 Chaui-Berlinck JG, Navas CA, Monteiro LHA, and Bicudo J. 2005. Control of metabolic rate is
764 a hidden variable in the allometric scaling of homeotherms. *Journal of Experimental*
765 *Biology* 208:1709-1716. 10.1242/jeb.01421

766 Costa M, Ghiran I, Peng CK, Nicholson-Weller A, and Goldberger AL. 2008. Complex

767 dynamics of human red blood cell flickering: alterations with in vivo aging. *Physical*
768 *Review E, Statistical, nonlinear, and soft matter physics* 78:020901.

769 Costa M, Goldberger AL, and Peng CK. 2002. Multiscale entropy analysis of complex
770 physiologic time series. *Physical Review Letters* 89:068102.

771 Darveau CA, Suarez RK, Andrews RD, and Hochachka PW. 2002. Allometric cascade as a
772 unifying principle of body mass effects on metabolism. *Nature* 417:166-170.
773 10.1038/417166a

774 Delignières D, and Torre K. 2009. Fractal dynamics of human gait: a reassessment of the 1996
775 data of Hausdorff et al. *Journal of Applied Physiology* 106:1272-1279.
776 10.1152/japplphysiol.90757.2008

777 Delignières, D., Torre, K., & Bernard, P. L. (2011). Transition from persistent to anti-persistent
778 correlations in postural sway indicates velocity-based control. PLoS Comput Biol, 7(2),
779 e1001089.

780 Eke, A., Herman, P., Bassingthwaighte, J. B., Raymond, G. M., Percival, D. B., Cannon, M., et
781 al. (2000). Physiological time series: Distinguishing fractal noises from motions. *Pflügers*
782 *Archives,* 439, 403–415.

783 Feder J. 1988. *Fractals*: Plenum Press.

784 Feldman DP, and Crutchfield JP. 1998. Measures of statistical complexity: Why? *Physics Letters*
785 *A* 238:244-252.

786 Glass L. 2001. Synchronization and rhythmic processes in physiology. *Nature* 410:277-284.
787 10.1038/35065745

788 Goldberger AL, Rigney DR, West BJ. Chaos and fractals in human physiology. Sci Am
789 1990;262:40–9.

790 Goldberger AL. Non-linear dynamics for clinicians: chaos theory, fractals, and complexity at the
791 bedside. Lancet 1996;347:1312–4.

792 Goldberger AL, Amaral LAN, Hausdorff JM, Ivanov PC, Peng CK, and Stanley HE. 2002.
793 Fractal dynamics in physiology: Alterations with disease and aging. *Proceedings of the*
794 *National Academy of Sciences of the United States of America* 99:2466-2472.
795 10.1073/pnas.012579499

796 Goldberger AL, and West BJ. 1987. Fractals in physiology and medicine. *The Yale journal of*
797 *biology and medicine* 60:421.

798 Gordon CJ. 2012. Thermal physiology of laboratory mice: Defining thermoneutrality. *Journal of*
799 *Thermal Biology* 37:654-685. http://dx.doi.org/10.1016/j.jtherbio.2012.08.004

800 Hausdorff JM, Ashkenazy Y, Peng CK, Ivanov PC, Stanley HE, and Goldberger AL. 2001.
801 When human walking becomes random walking: fractal analysis and modeling of gait
802 rhythm fluctuations. *Physica A* 302:138-147. 10.1016/s0378-4371(01)00460-5

803 Hochachka PW, Darveau CA, Andrews RD, and Suarez RK. 2003. Allometric cascade: a model
804 for resolving body mass effects on metabolism. *Comparative biochemistry and*
805 *physiology Part A, Molecular & integrative physiology* 134:675-691. 10.1016/s1095-

6433(02)00364-1

Hu K, Ivanov PC, Chen Z, Hilton MF, Stanley HE, and Shea SA. 2004. Non-random fluctuations and multi-scale dynamics regulation of human activity. *Physica A* 337:307-318. 10.1016/j.physa.2004.01.042

Humeau A, Buard B, Chapeau-Blondeau F, Rousseau D, Mahe G, and Abraham P. 2009. Multifractal analysis of central (electrocardiography) and peripheral (laser Doppler flowmetry) cardiovascular time series from healthy human subjects. *Physiological Measurement* 30:617-629. 10.1088/0967-3334/30/7/007

Hurst HE. 1951. Long-term storage capacity of reservoirs. *T Am Soc CIiv Eng* 116:770-799.

Ihlen, EA. 2012. Introduction to multifractal detrended fluctuation analysis in Matlab. *Frontiers in Physiology*, 3:141.x1-141.18 . 10.3389/fphys.2012.00141

Ivanov PC, Amaral LAN, Goldberger AL, Havlin S, Rosenblum MG, Struzik ZR, and Stanley HE. 1999. Multifractality in human heartbeat dynamics. *Nature* 399:461-465. 10.1038/20924

Ivanov PC, Hu K, Hilton MF, Shea SA, and Stanley HE. 2007. Endogenous circadian rhythm in human motor activity uncoupled from circadian influences on cardiac dynamics. *Proceedings of the National Academy of Sciences of the United States of America* 104:20702-20707.

Kantelhardt JW. 2011. Fractal and multifractal time series. In: Meyer RA, ed. *Mathematics of Complexity and Dynamical Systems*. New York: Springer, 463-487.

826 Kantelhardt JW, Koscielny-Bunde E, Rybski D, Braun P, Bunde A, and Havlin S. 2006. Long-
827 term persistence and multifractality of precipitation and river runoff records. *Journal of*
828 *geophysical research Atmospheres : JGR* 111. D01106

829 10.1029/2005jd005881

830 Kantelhardt JW, Rybski D, Zschiegner SA, Braun P, Koscielny-Bunde E, Livina V, Havlin S,
831 and Bunde A. 2003. Multifractality of river runoff and precipitation: comparison of
832 fluctuation analysis and wavelet methods. *Physica A* 330:240-245.
833 10.1016/j.physa.2003.08.019

834 Kantelhardt JW, Zschiegner SA, Koscielny-Bunde E, Havlin S, Bunde A, and Stanley HE. 2002.
835 Multifractal detrended fluctuation analysis of nonstationary time series. *Physica A*
836 316:87-114. Pii s0378-4371(02)01383-3

837 10.1016/s0378-4371(02)01383-3

838 Karasov WH, and Rio CM. 2007. *Physiological ecology: how animals process energy, nutrients,*
839 *and toxins*: Princeton University Press.

840 Koscielny-Bunde E, Kantelhardt JW, Braun P, Bunde A, and Havlin S. 2006. Long-term
841 persistence and multifractality of river runoff records: Detrended fluctuation studies.
842 *Journal of Hydrology* 322:120-137. 10.1016/j.jhydro1.2005.03.004

843 Labra FA, Marquet PA, and Bozinovic F. 2007. Scaling metabolic rate fluctuations. *Proceedings*
844 *of the National Academy of Sciences of the United States of America* 104:10900-10903.
845 10.1073/pnas.0704108104

Lighton JRB. 2008. *Measuring metabolic rates: a manual for scientists*: Oxford University Press.

Lipsitz LA. 2004. Physiological complexity, aging, and the path to frailty. *Science of aging knowledge environment : SAGE KE* 2004:pe16. 10.1126/sageke.2004.16.pe16

Ludescher J, Bogachev MI, Kantelhardt JW, Schumann AY, and Bunde A. 2011. On spurious and corrupted multifractality: The effects of additive noise, short-term memory and periodic trends. *Physica A* 390:2480-2490. 10.1016/j.physa.2011.03.008

Mantegna RN, and Stanley HE. 1997. Econophysics: Scaling and its breakdown in finance. *Journal of Statistical Physics* 89:469-479. 10.1007/bf02770777

Mantegna RN, and Stanley HE. 2000. *An Introduction to Econophysics: Correlations and Complexity in Finance*: Cambridge University Press.

McNab BK. 2002. *The physiological ecology of vertebrates: a view from energetics*: Cornell University Press.

Muggeo, V. 2003. Estimating regression models with un-known break-points. Statistics in Medicine, 22: 3055–3071.

Oswiecimka P, Kwapien J, and Drozdz S. 2006. Wavelet versus detrended fluctuation analysis of multifractal structures. *Physical Review E, Statistical, nonlinear, and soft matter physics* 74. 01610310.1103/PhysRevE.74.016103

Peng CK, Buldyrev SV, Goldberger AL, Havlin S, Mantegna RN, Simons M, and Stanley HE.

1995a. Statistical properties of DNA-sequences. *Physica A* 221:180-192. 10.1016/0378-4371(95)00247-5

Peng CK, Havlin S, Stanley HE, and Goldberger AL. 1995b. Quantification of scaling exponents and crossover phenomena in nonstationary heartbeat time-series. *Chaos* 5:82-87. 10.1063/1.166141

Peng CK, Mietus J, Hausdorff JM, Havlin S, Stanley HE, and Goldberger AL. 1993. Long-range anticorrelations and non-gaussian behavior of the heartbeat. *Physical Review Letters* 70:1343-1346. 10.1103/PhysRevLett.70.1343

Peng CK, Mietus JE, Liu Y, Lee C, Hausdorff JM, Stanley HE, Goldberger AL, and Lipsitz LA. 2002. Quantifying fractal dynamics of human respiration: age and gender effects. *Annals of Biomedical Engineering* 30:683-692.

Pincus SM. 1991. Approximate entropy as a measure of system complexity. *Proceedings of the National Academy of Sciences* 88:2297-2301.

R Core Team (2014). R: A language and environment for statistical computing. R Foundation for Statistical Computing, Vienna, Austria. URL http://www.R-project.org/.

Rezek IA, and Roberts SJ. 1998. Stochastic complexity measures for physiological signal analysis. *IEEE Transactions on Biomedical Engineering* 45:1186-1191.

Richman JS, and Moorman JR. 2000. Physiological time-series analysis using approximate entropy and sample entropy. *American Journal of Physiology-Heart and Circulatory Physiology* 278:H2039-H2049.

885 Schaefer, A., Brach, J. S., Perera, S., & Sejdić, E. (2014). A comparative analysis of spectral
886 exponent estimation techniques for $1/f^{\beta}$ processes with applications to the analysis of
887 stride interval time series. Journal of neuroscience methods, 222, 118-130.

888 Schreiber T, and Schmitz A. 1996. Improved surrogate data for nonlinearity tests. *Physical*
889 *Review Letters* 77:635-638. 10.1103/PhysRevLett.77.635

890 Schreiber T, and Schmitz A. 2000. Surrogate time series. *Physica D* 142:346-382.
891 10.1016/s0167-2789(00)00043-9

892 Spicer J, and Gaston K. 2009. *Physiological Diversity: Ecological Implications*: Wiley. com.

893 Suki B, Alencar AM, Frey U, Ivanov PC, Buldyrev SV, Majumdar A, Stanley HE, Dawson CA,
894 Krenz GS, and Mishima M. 2003. Fluctuations, noise and scaling in the cardio-
895 pulmonary system. *Fluct N Lett* 3:R1-R25. 10.1142/s0219477503001142

896 Weibel ER, Bacigalupe LD, Schmitt B, and Hoppeler H. 2004. Allometric scaling of maximal
897 metabolic rate in mammals: muscle aerobic capacity as determinant factor. *Respiratory*
898 *physiology & neurobiology* 140:115-132. 10.1016/j.resp.2004.01.006

899 West BJ, Bassingthwaighte JB, and Liebovitch LS. 1994. *Fractal physiology*: Oxford University
900 Press.

901 West BJ, and Scafetta N. 2003. Nonlinear dynamical model of human gait. *Physical review E* 67.
902 051917.10.1103/PhysRevE.67.051917

903 West, B. J., & Shlesinger, M. F. (1989). On the ubiquity of 1/f noise. International Journal of

Modern Physics B, 3(06), 795-819.

Witt, A., & Malamud, B. D. (2013). Quantification of long-range persistence in geophysical time series: conventional and benchmark-based improvement techniques. Surveys in Geophysics, 34(5), 541-651.

910

911

Figure 1 (on next page)

Long-term correlations of metabolic rate fluctuations in *Mus musculus*.

(a) Average metabolic rates (VO_2) measured at different ambient temperatures. Average values ± standard errors are shown with open circles and error bars. Straight line shows calculated thermal conductance, while the humped curve corresponds to a fitted three parameter Gaussian function (g(x)=a*exp(-.5*((x-x0)/b)^2)). (b) Metabolic rate (VO_2) time series shown for a representative individual measured at 30ºC for 1 ¾ hours at 1(s) intervals. Note the irregular, nonstationary dynamics, despite thermo neutral ambient temperature. (c) Observed VO_2 fluctuations $r(VO2)=log10[VO_2\ (t+1)/\ VO_2\ (t)]$ time series for data in (b). Note the clustering of broad and narrow fluctuations. (d) Randomized $r(VO_2)$ values, showing the loss of the clustering of fluctuations. (e) Fourier power spectra for time series in (c) and (d) shown by blue and red lines respectively. A smoothing procedure was applied, which consisted of averaging the spectra for consecutive overlapping segments of 256 data points. Fitted OLS scaling relationships are shown in dotted lines. (f) Detrended fluctuation analyses (DFA) for the two time series shown in (c) and (d). Fluctuation functions for original and shuffled time series in are shown in open and filled circles respectively. Fitted scaling relationships are shown in dashed lines. Note the change in exponent values above s=100 for the original time series.

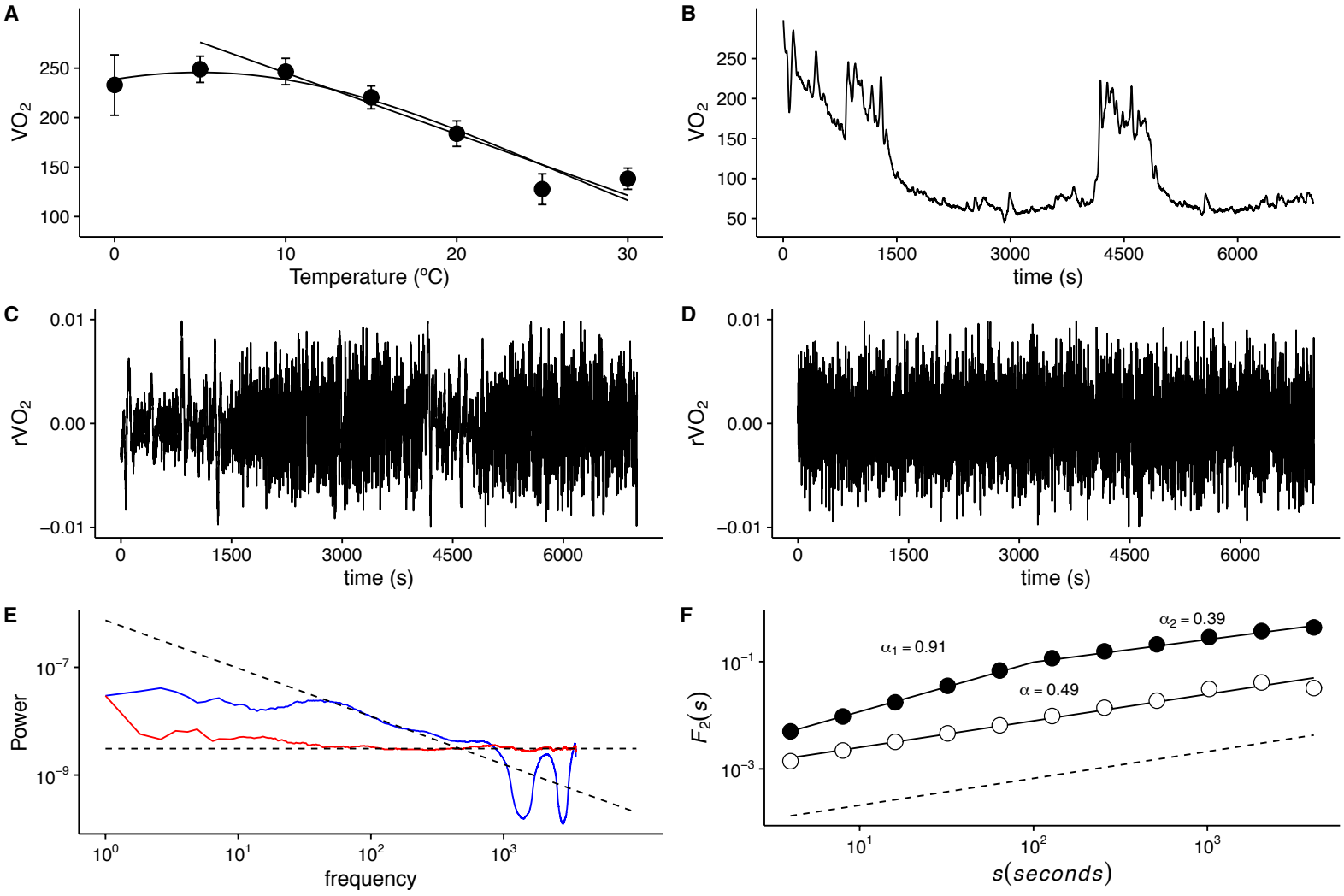

Figure 2 (on next page)

Temperature effects on root-mean-square fluctuation function of $r(VO_2)$ in mice.

The figure shows the average $F_2(s)$ functions calculated with linear detrending for all mice. Results for the time series studied at 30ºC, 20ºC, 10ºC and 0ºC are shown in the respective columns arranged from left to right. Figures (a) to (d) show the average DFA functions calculated for the $r(VO_2)$ time series, while figures (e) to (h) show average DFA functions calculated for the AAFT shuffled data. All figures show the DFA root-mean-square fluctuation functions obtained using three different orders of detrending polynomials: linear (open circles), quadratic (open squares) and cubic functions (open triangles). Two scaling regimes can be observed across all temperatures and for all polynomial detrending orders. The first scaling regime spans scales between 8 and 100 s, while the second one spans scales from 100 to 1024 s. All curves have been shifted vertically for clarity. Please note that while only four experimental temperatures are shown, the remaining three temperatures show similar patterns.

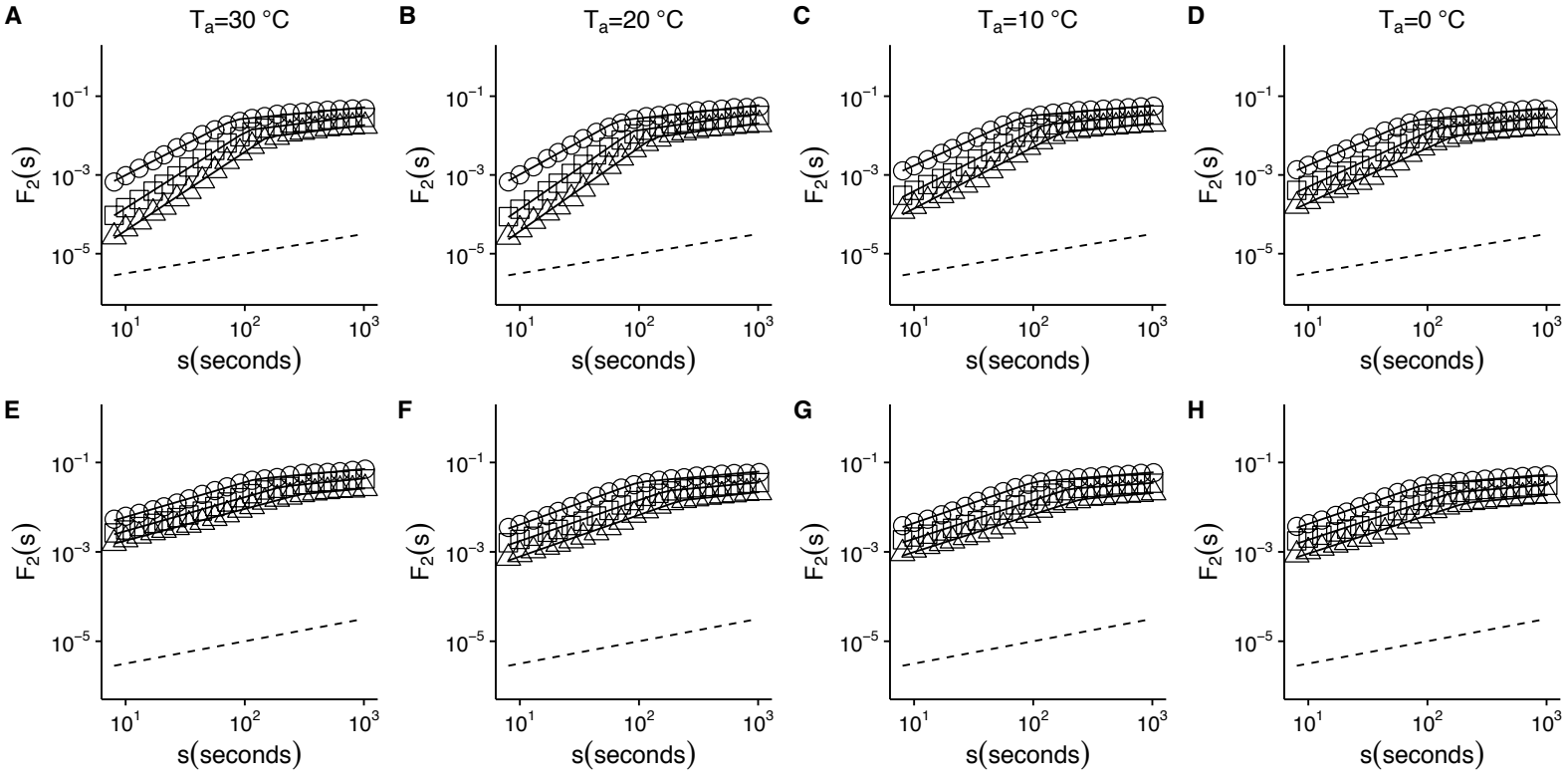

Figure 3(on next page)

Temperature effects on long range scaling exponent α in metabolic rate fluctuations.

The figure shows the average DFA scaling exponent α_{DFA} calculated as a function of experimental temperature. Average scaling exponents corresponding to exponent for raw *r(VO2)* data within the $10 < s < 100$ scaling regime are shown with filled circles, while filled squares show the scaling exponents for the raw *r(VO2)* data within the $100 < s < 1024$ scaling regimes are shown with.

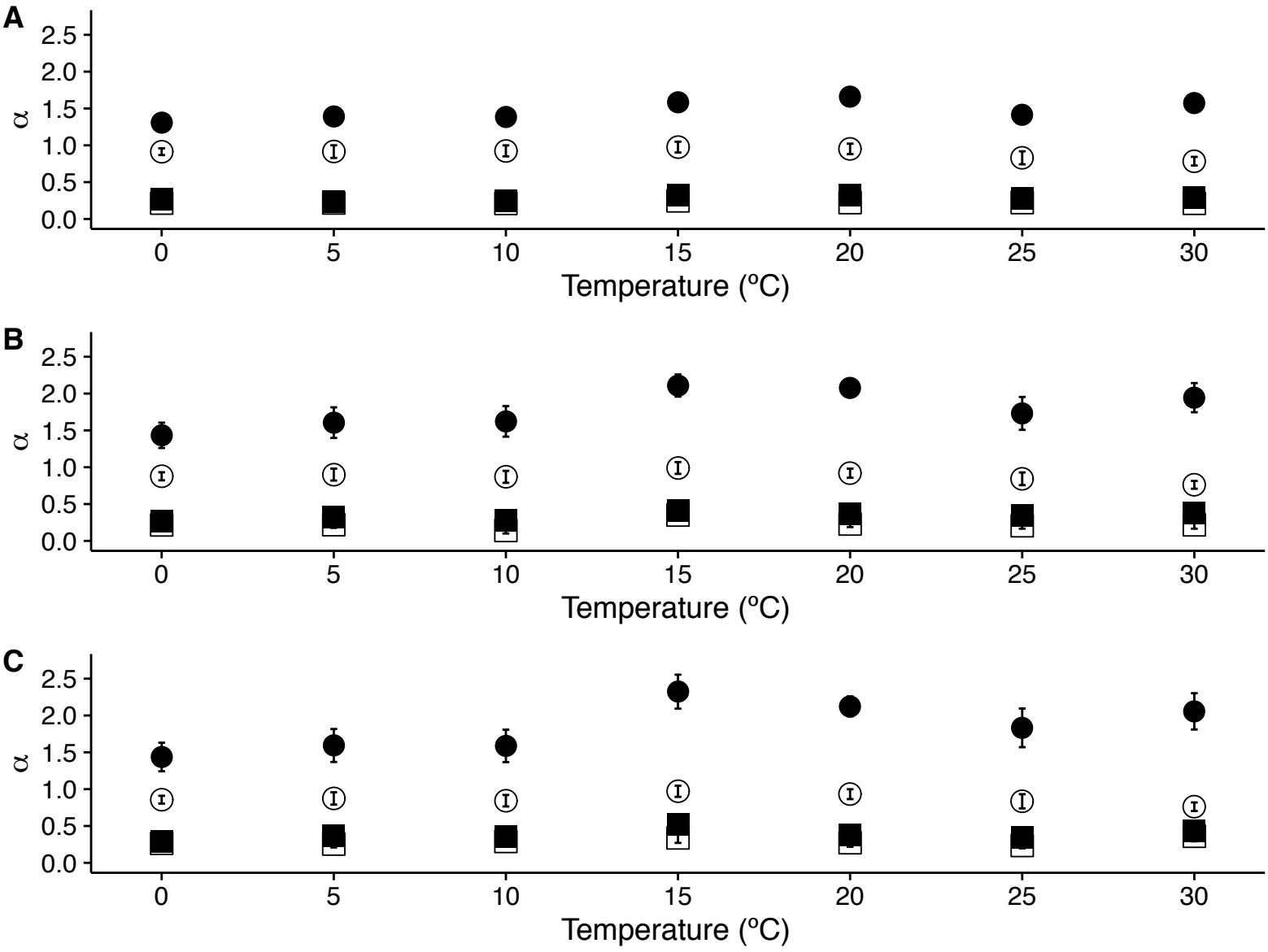

PeerJ Preprints | https://doi.org/10.7287/peerj.preprints.2404v1 | CC BY 4.0 Open Access | rec: 1 Sep 2016, publ: 1 Sep 2016

Figure 4(on next page)

Local DFA scaling exponents.

The Figure shows the value of local DFA scaling exponents α_{DFA} for the time series in figures 1c (blue lines) and 1d (red lines). Local exponents are calculated with a moving window shifted across the whole time series. Figures (a), (b) and (c) show the results for shifting window widths of 128, 256 and 512 seconds respectively. The heterogeneity of the rate of change in metabolic rate is revealed by the broad range of local scaling exponents α_{DFA}, which shows a complex structure in time as opposed to the simpler and more restricted changes in the shuffled time series.

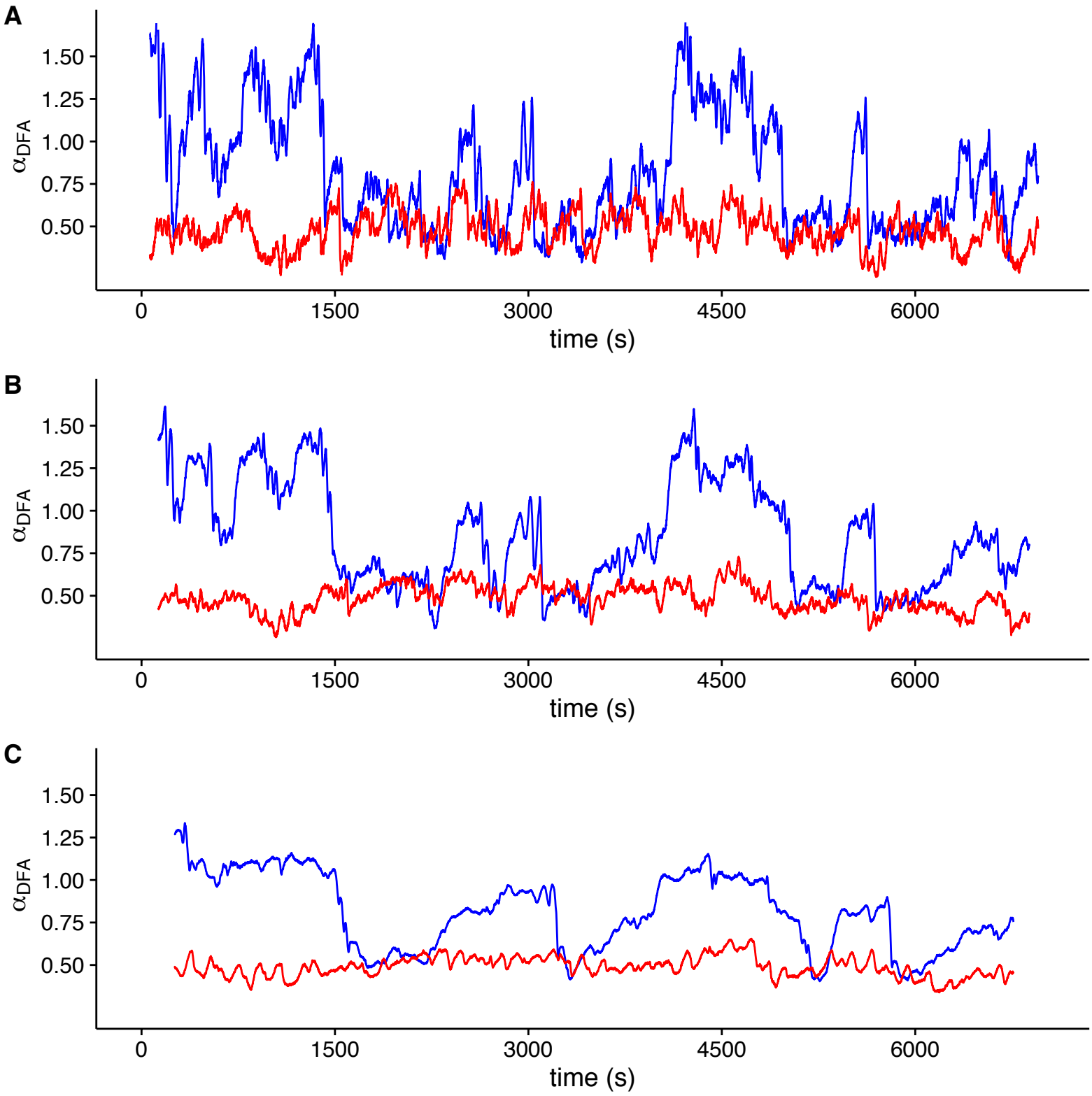

PeerJ Preprints | https://doi.org/10.7287/peerj.preprints.2404v1 | CC BY 4.0 Open Access | rec: 1 Sep 2016, publ: 1 Sep 2016

Figure 5 (on next page)

Temperature effects on generalized fluctuation function of $r(VO_2)$ in mice.

Figure shows log-log plots of the average generalized fluctuation function $F_q(s)$ as a function of time s in $r(VO2)$ time series. Columns left to right show the results for $F_q(s)$ functions calculated for 30ºC, 20ºC, 10ºC and 0ºC respectively. Figures (a) to (d) show the average $F_q(s)$ functions calculated for the $r(VO_2)$ time series, while figures (e) to (h) show average $F_q(s)$ functions calculated for the AAFT shuffled data. Open circles in all figures show the observed $F_q(s)$ values for different values of q, with q = 8, 4, 2,1,0, -1,-2, -4, and -8 (from the top to the bottom). Also shown in black lines are piecewise linear regression fits to the $F_q(s)$ functions. Dashed straight lines with slope h = 0.5 are shown below the data in each figure to allow qualitative comparison with the uncorrelated case. Please note that while only four experimental temperatures are shown, the remaining three temperatures show similar patterns.

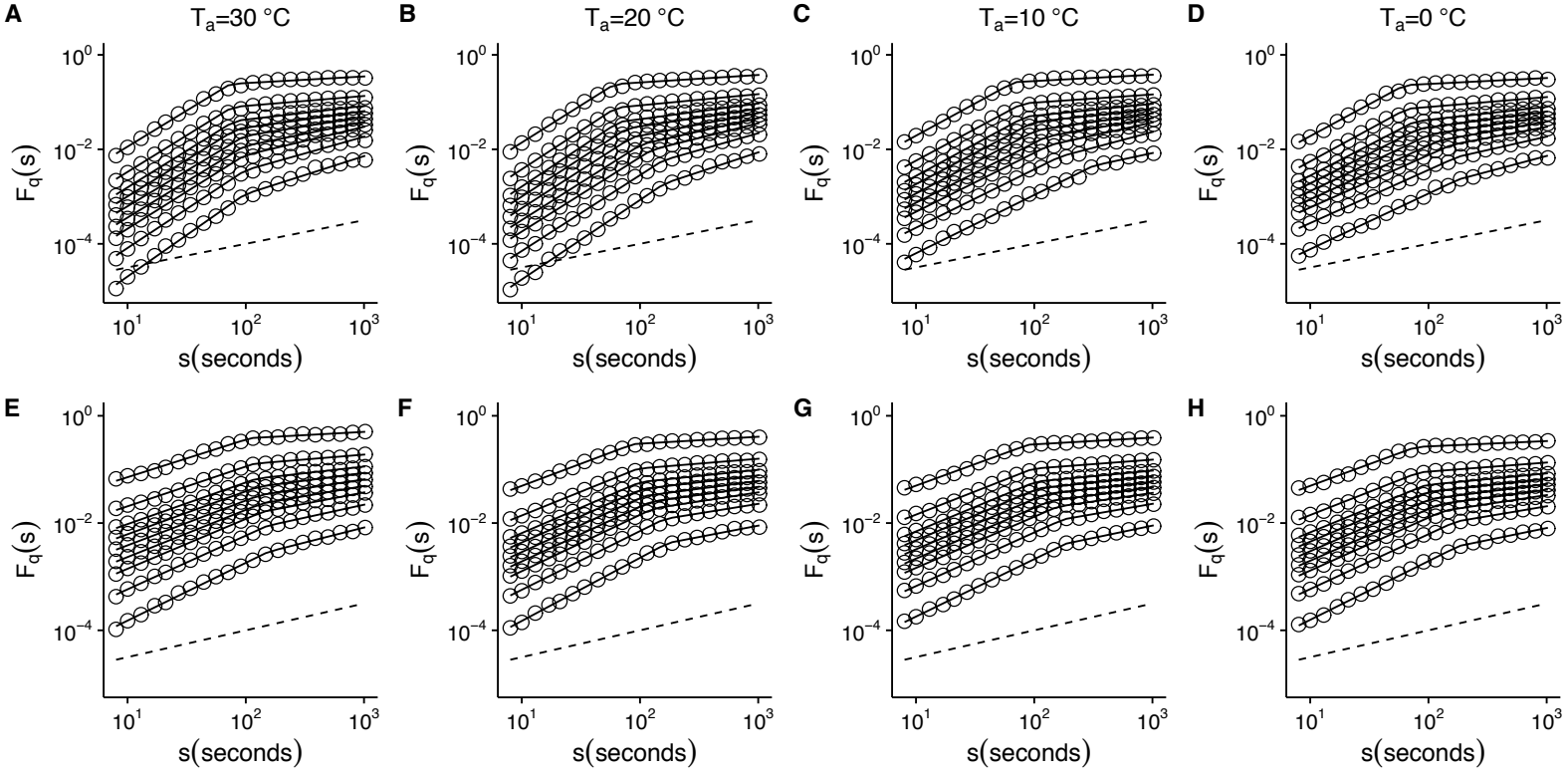

Figure 6(on next page)

Multifractal Detrended Fluctuation Analysis of *Mus musculus r(VO2)* time series across different temperature treatments.

The figure shows the results of the multifractal scaling analysis for all mice studied. Left, central and right hand column show the results for the generalized Hurst exponent spectra (*h(q)*), Renyi exponent spectra (*τ(q)*) and singularity spectra (*f(α)*). Each figure shows in dashed and continuous black lines the smoothed conditional mean of the different spectra for the first and second scaling regimes respectively. For shuffled data, the smoothed conditional mean of the different spectra for the first and second scaling regimes are shown by dashed and continuous red lines respectively. For figures (c), (f) and (i), the singularity spectra of the first regime corresponds to a single point, shown by a filled circle. The singularity spectra reveal that for temperatures in the range 0ºC < T_a <1 0ºC the time scales in the 8 < s < 100 range present a monofractal scaling, while all remaining temperatures show a weak multifractal scaling. All data for the second scaling regime show strong multifractality, which is not completely lost when data are shuffled.

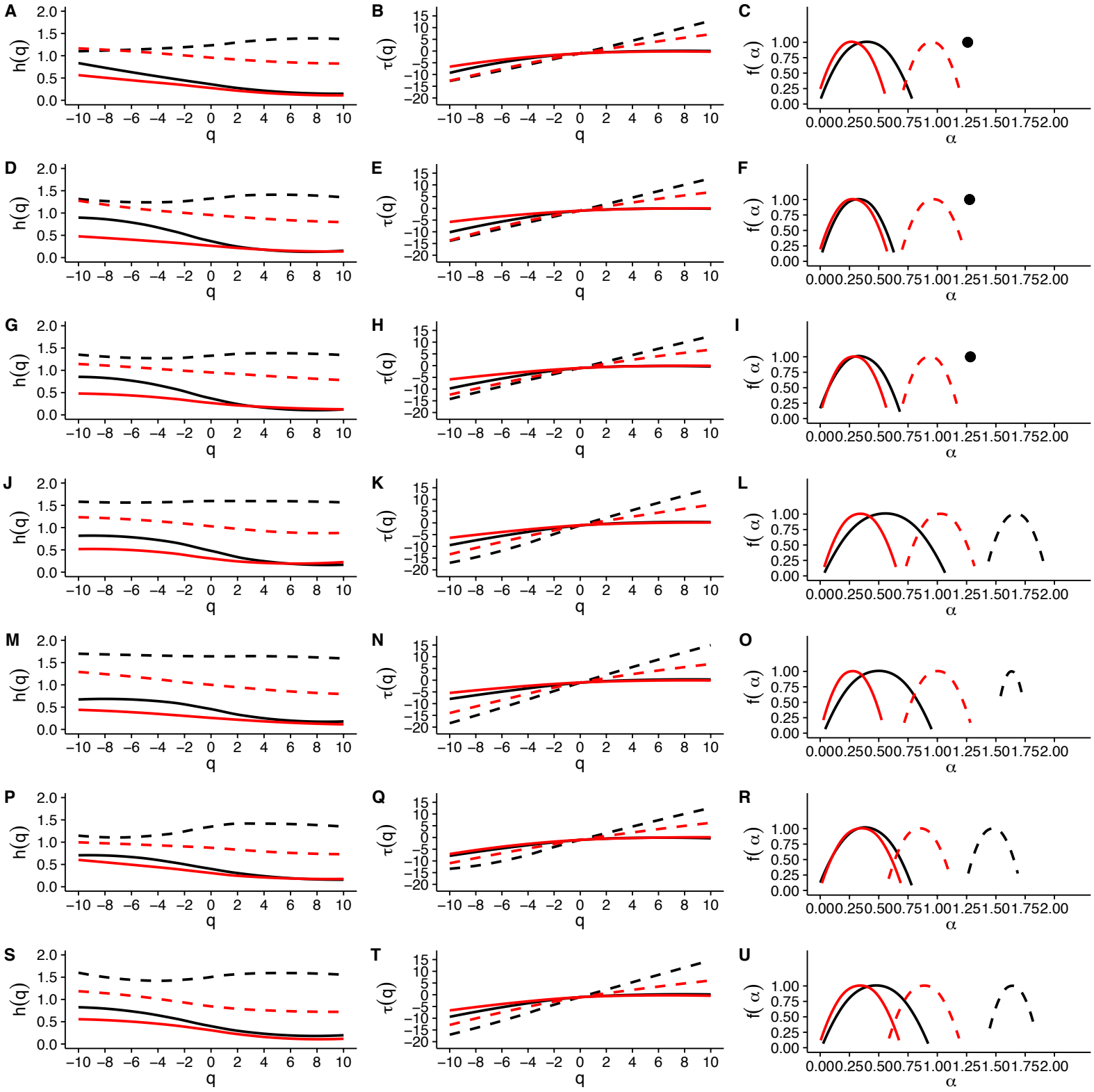

Figure 7 (on next page)

Temperature effects on the strength of multifractality in mice.

The figure shows the average widths $\Delta\alpha$, of the $f(\alpha)$ spectra as a function of environmental temperature T_a. Left hand, central and right hand columns show the results for linear, quadratic and cubic polynomial de-trending respectively. Figures (a) to (d) show the average $\Delta\alpha$ values calculated for the $r(VO_2)$ time series, while figures (e) to (h) show the average $\Delta\alpha$ values calculated for the AAFT shuffled data.

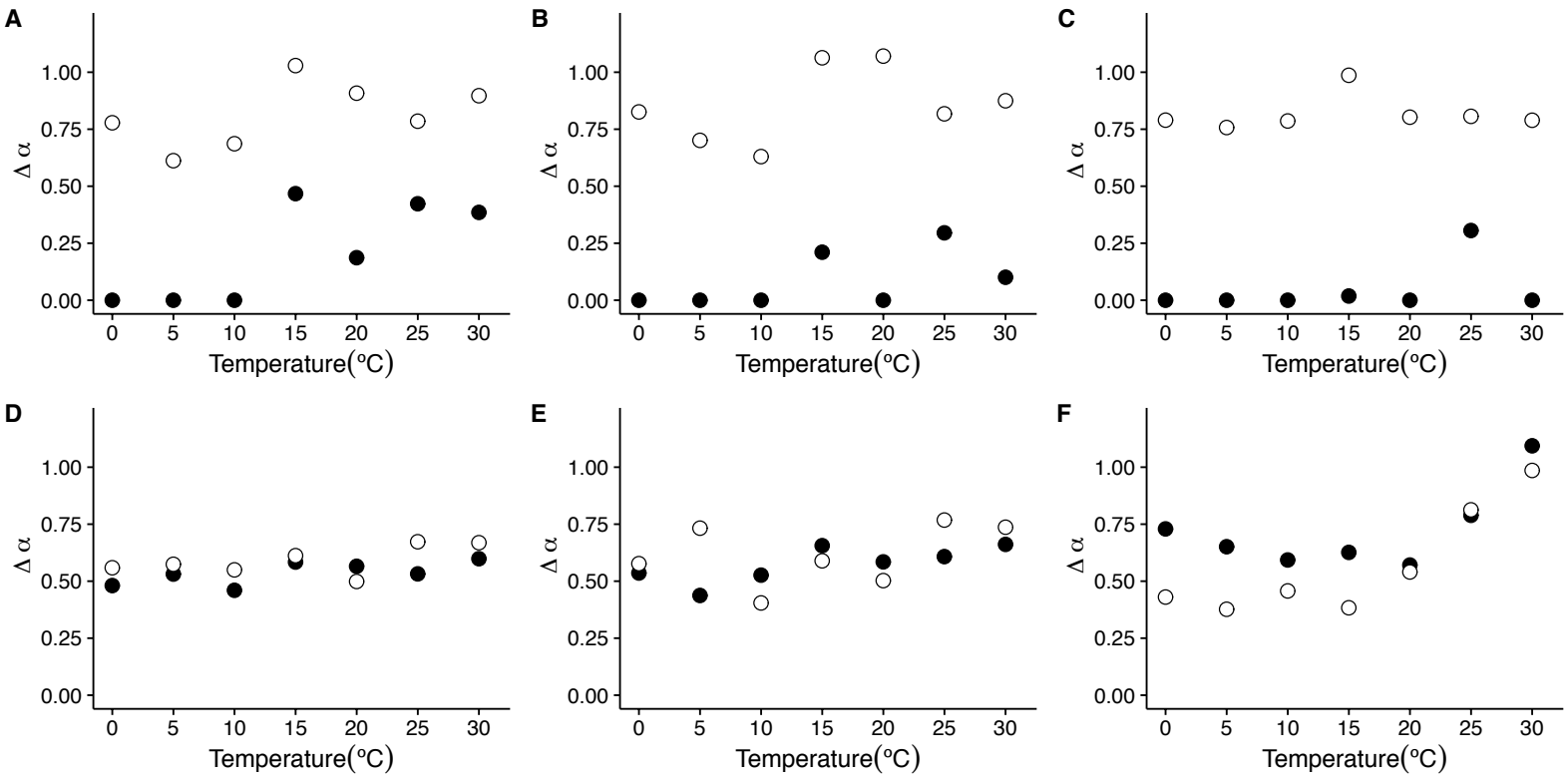

Figure 8(on next page)

Temperature effects on the dominant multifractal exponent in mice.

Temperature effects on the dominant multifractal exponent in *Mus musculus*. The figure shows the average dominant fractal exponent α_{max}, for the different the $f(\alpha)$ spectra as a function of environmental temperature T_a. The left hand, central and right hand columns show the results for linear, quadratic and cubic polynomial detrending respectively. Figures (a) to (d) show the average α_{max} values calculated for the $r(VO_2)$ time series, while figures (e) to (h) show the average α_{max} values calculated for the AAFT shuffled data.